Abdominal Radiology

Published online: 25 June 2018

Abdom Radiol (2019) 44:154–179
https://doi.org/10.1007/s00261-018-1670-5

Bilateral adrenal abnormalities: imaging review of different entities

Meshal Ali Alshahrani,[1] Mnahi Bin Saeedan,[1] Tariq Alkhunaizan,[1] Ibtisam Musallam Aljohani,[1] and Fahad Mohammed Azzumeea[2]

[1]Department of Radiology, King Faisal Specialist Hospital and Research Center, MBC-28, P.O. Box 3354, Riyadh 11211, Saudi Arabia
[2]National Guard Health Affairs, King Abdulaziz Medical City, Medical Imaging Department, Riyadh, Saudi Arabia

Abstract

Bilateral adrenal abnormalities are not infrequently encountered during routine daily radiology practice. The differential diagnoses of bilateral adrenal abnormalities include neoplastic and non-neoplastic entities. The bilateral adrenal tumors include metastasis, lymphoma, neuroblastoma, pheochromocytoma, adenoma, and myelolipoma. Non-neoplastic bilateral adrenal masses include infectious processes and haematomas. There are different diffuse bilateral adrenal changes such as adrenal atrophy, adrenal enlargement, adrenal calcifications, and altered adrenal enhancement. In this pictorial review article, we will discuss the imaging features of these entities with emphasis on their clinical implications.

Key words: Bilateral adrenal—Adrenal adenoma—Metastasis—Lymphoma—Pheochromocytoma—Neuroblastoma—Tuberculosis—Hematoma—Adrenal hyperplasia—Addison—Wolman—Hypoperfusion complex—Adrenal infarction

The advancement and the wide availability of cross-sectional imaging have resulted in substantial increases in the number of incidentally detected adrenal lesions. Adrenal lesions are detected in about 4% of abdominal CT scans obtained for different indications. The prevalence of detected adrenal lesion increases to approximately 10% among the elderly [1]. Most of these lesions are unilateral and benign non-functioning adrenal adenomas, representing the vast majority of such unilateral lesions [2, 3]. Although adrenal lesions are commonly asymptomatic on presentation, the endocrinology literature recommends further clinical evaluation and hormonal workup to assess for subclinical Cushing syndrome, hyperaldosteronism, or pheochromocytoma. Workup assessment includes urine or plasma metanephrines, plasma aldosterone concentration-to-plasma renin ratio, and a 1-mg dexamethasone suppression test [4, 5].

17% and 23% of incidentally detected adrenal lesions were reported to be bilateral [5, 6]. The differential diagnosis of bilateral adrenal abnormalities includes malignant and benign tumors, and different non-neoplastic entities. The bilaterality may narrow the differential diagnoses as bilateral adrenal lesions, being more likely to represent metastases, lymphomas, and granulomatous diseases, such as tuberculosis. In the case of trauma or history of bleeding tendency, bilateral adrenal hemorrhage is also a differential consideration. Pheochromocytoma and neuroblastoma can be bilateral, which should raise the possibility of genetic predisposition or familial syndromes.

Diffuse adrenal changes can be seen in different entities, including adrenal atrophy in Addison's disease, adrenal enlargement in adrenal hyperplasia, diffuse adrenal calcifications in Wolman's disease, intense adrenal enhancement in the hypoperfusion complex, and reduced enhancement in adrenal infarction [7–9]. In this article, we will review multi-modality imaging appearances of these entities with emphasis on their clinical implications.

Electronic supplementary material The online version of this article (https://doi.org/10.1007/s00261-018-1670-5) contains supplementary material, which is available to authorized users.

Correspondence to: Mnahi Bin Saeedan; *email:* mbinsaeedan@gmail.com

Adrenal tumors and mass-like lesions

Adenoma

About 75% of incidentally discovered adrenal lesions are adenomas and 78% of these are lipid rich [3]. The majority of adrenal adenomas are non-functioning and about 20% are bilateral [3, 10]. Adrenal adenoma with enlargement of the rest of the adrenal gland parenchyma is suggestive of functioning adenoma with adrenal hyperplasia [11, 12]. In one study, bilateral adrenal adenomas and adrenal adenoma on one side with contralateral non-adenomatous lesion represented the majority of incidentally detected bilateral adrenal lesions. It also showed a higher incidence of subclinical Cushing syndrome as compared to patients with unilateral incidental adrenal lesions [5]. Adrenal vein sampling helps in localizing the side of hormone-secreting adenoma in the case of bilateral adrenal adenoma. This will subsequently determine the side of surgical resection [13].

An incidentally detected adrenal lesion in a patient with no known malignancy is likely to be an adenoma. If there is no previous imaging to document stability, further evaluation should be performed with chemical shift magnetic resonance imaging (CS-MRI) or non-contrast CT. The CS-MRI is preferred because it is slightly more accurate and carries no radiation hazard [14, 15]. The typical imaging features of adrenal adenoma include small size (usually < 4 cm), homogeneous internal texture, well-defined margins, intracellular fat, and washout on a dedicated adrenal CT protocol. A cut-off of less than 10 HU on a non-enhanced CT scan is generally used to diagnose adrenal adenoma (Fig. 1). The proper measurement of the adrenal lesion attenuation value on non-enhanced CT is performed by placing a region of interest over one-half to two-thirds of the adrenal lesion to avoid noise-related sampling [3, 16].

Loss of signal seen on CS-MRI is due to the presence of intra-cellular fat. The precession frequency of fat and water protons is different. During in-phase (IP) imaging, fat and water proton signals are aligned. During opposed-phase (OP) imaging, the fat and water signals are opposite to each other, resulting in signal cancelation and signal drop in both water and fat protons within the same voxel (Fig. 2). Adrenal lesion signal loss is usually assessed subjectively. Objective measures such as the adrenal-to-spleen chemical shift ratio (ASR) or the adrenal sensitivity index can be used. Subtraction techniques (Subtracted images = OP images − IP images) can improve the qualitative evaluation [14, 17].

Some of the indeterminate adrenal lesions in the non-contrast CT (HU 10–30) will show drop in the out phases. Adrenal lesions with HU more than 43 on non-contrast CT are suspicious for malignancy and less likely to represent adrenal adenoma [14, 15]. Some of the adrenal adenomas are indeterminate on both non-contrast CT (HU > 10) and CS-MRI (no signal drop in the opposed phase images). The adrenal CT protocol is the proper diagnostic imaging choice for such indeterminate cases. Adrenal adenomas tend to enhance rapidly with a rapid loss of contrast medium "contrast washout," unlike most malignant lesions which enhance rapidly and usually show a slower washout. The adrenal mass CT protocol includes a pre-contrast scan, a portal venous phase (70 seconds) scan, and a 15-minute delay scan. The absolute percentage washout (APW) is derived from the

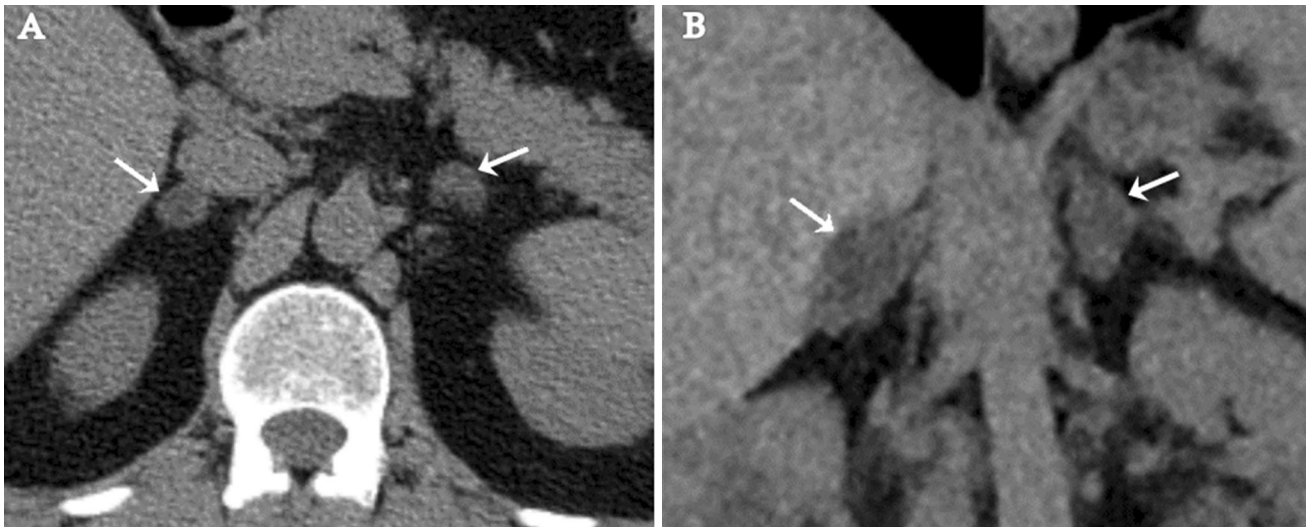

Fig. 1. Incidentally detected bilateral adrenal adenomas. Axial non-enhanced CT image (**A**) shows bilateral low attenuation adrenal nodules (arrows). The right adrenal nodule has an attenuation of − 6 HU and the left adrenal nodule has an attenuation of 6 HU, consistent with lipid-rich adrenal adenomas. Coronal non-enhanced CT image (**B**) of a different patient shows bilateral homogenous adrenal nodules (arrows) of low attenuation (− 10 HU), consistent with lipid-rich adrenal adenomas.

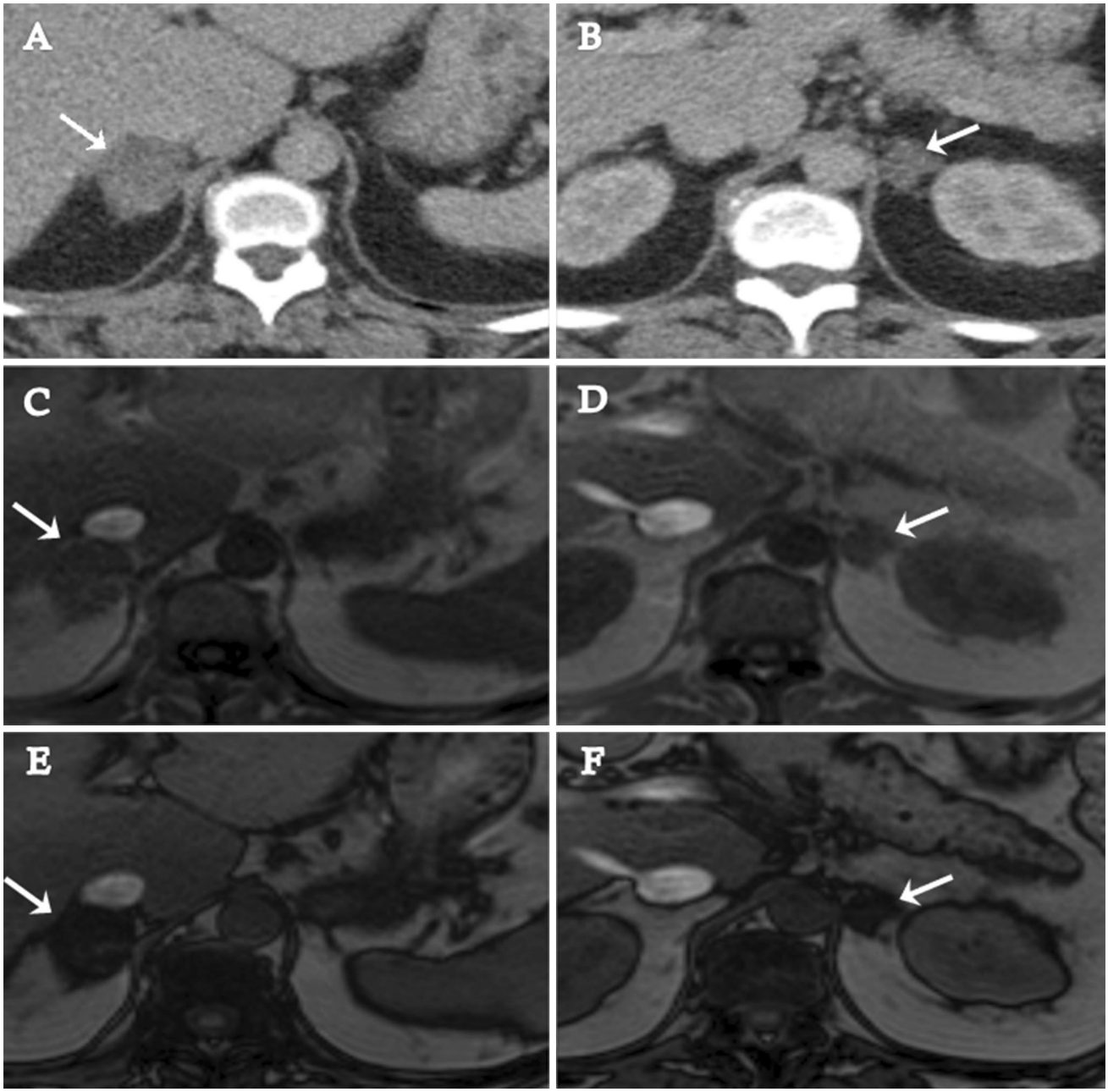

Fig. 2. 55-year-old woman with renal cell carcinoma and bilateral adrenal adenomas. Axial contrast-enhanced CT images in portal venous phase (**A**, **B**) show bilateral homogenous adrenal nodules (HU = 30). Abdominal MRI in-phase T1 (**C**, **D**) and out-phase T1 weighted images (**E**, **F**) show homogenous signal drop of both adrenal nodules in the out-phase images, consistent with bilateral adrenal adenomas.

following: ([enhanced HU − delayed HU]/[enhanced HU − non-contrast HU]) × 100. An APW value of 60% or greater is diagnostic of an adenoma. In the absence of unenhanced series, the relative percentage washout (RPW) can be used and derived from: ([enhanced HU − delayed HU]/enhanced HU) × 100. An RPW value greater than 40% is diagnostic of adenoma. Adrenal contrast washout is not affected by the lesion intracellular fat content and allows confident diagnosis of both lipid-rich and lipid-poor adenoma [14, 15, 18].

Bilateral adrenal adenomas and unilateral adrenal adenoma with contralateral benign or malignant adrenal lesion should be considered as well when radiologists encounter bilateral adrenal lesions. (Figs. 3 and 4). Therefore, each adrenal lesion should be fully assessed independently form the other contralateral adrenal lesions. It is important to know that clear cell renal cell carcinoma (RCC) and hepatocellular carcinoma (HCC) metastases may contain intercellular fat and may show washout [19–21]. However, imaging features with no

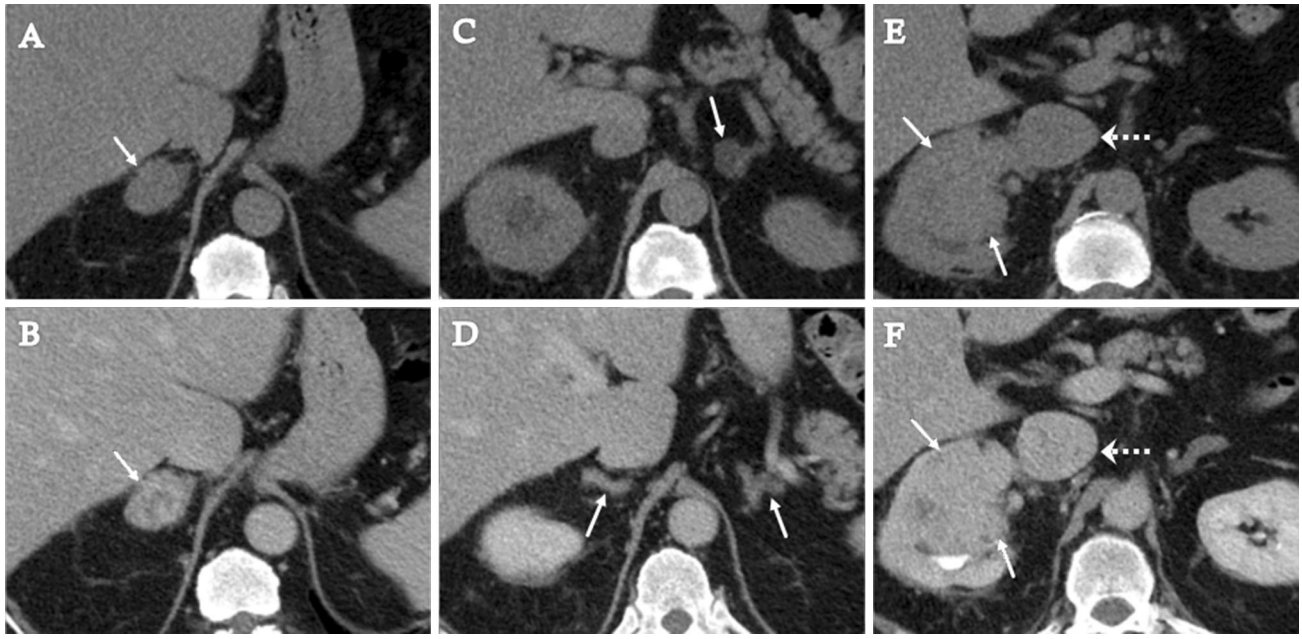

Fig. 3. 72-year-old man with right renal cell carcinoma, IVC invasion, right adrenal metastasis, and left adrenal adenoma. Axial non-enhanced (**A**) and contrast-enhanced (**B**) CT images show a heterogeneously enhancing right adrenal lesion (arrows). Axial non-enhanced CT image (**C**) shows a small homogenous left adrenal lesion of − 30 HU (arrow), consistent with lipid-rich adrenal adenoma. Axial contrast-enhanced CT image (**D**) shows bilateral adrenal enlargement (arrows), suggestive of adrenal hyperplasia. Axial non-enhanced (**E**) and contrast-enhanced (**F**) CT images show a heterogeneously enhancing right renal lesion (arrows), and enlarged IVC with enhancing tumor thrombus (dashed arrows). A two-year follow-up (not shown) after right adrenalectomy and nephrectomy shows stable left adrenal adenoma with no signs of disease recurrence.

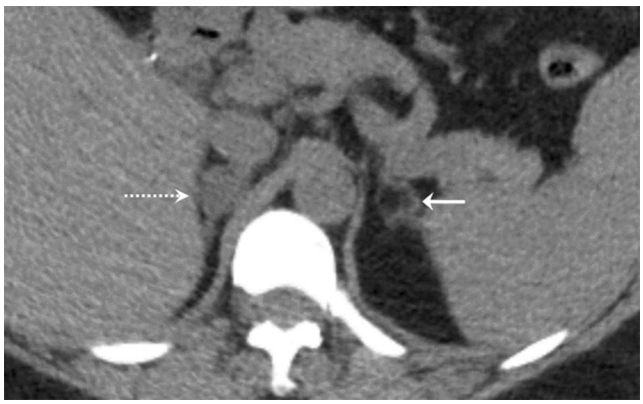

Fig. 4. Incidentally detected bilateral adrenal lesions. Axial non-enhanced CT image shows a right adrenal lesion of low attenuation (10 HU) consistent with adrenal adenoma (dashed arrow), and a left adrenal lesion with macroscopic fat consistent with myelolipoma (solid arrow).

known primary malignancy are highly suggestive of adrenal adenoma.

Metastasis

The adrenal gland is a fertile site for metastases from lung, breast, gastric, renal, pancreatic, and colon carcinomas; melanomas and malignant lymphomas. Bilateral adrenal metastases were reported in almost half of the patients with pathologically proven adrenal metastasis [22]. Incidental adrenal metastasis from unknown malignancy is exceedingly rare [3]. Therefore, bilateral adrenal metastases are usually diagnosed by imaging with a high degree of certainty in the presence of known malignancy without need for biopsy and pathology confirmation. Patients with bilateral metastases are at a higher risk of adrenal insufficiency, and therefore clinical attention to such a possible complication is needed. The detection of adrenal metastasis in patients with primary malignancy indicates an advanced stage. However, surgical resection of adrenal metastasis may improve long-term survival in some cases (Fig. 3) [22].

The differentiation of metastatic disease from adrenal adenoma in a patient with primary malignancy is critical. Adrenal metastasis attenuation value is greater than 10 HU on unenhanced CT [16]. The presence of intracellular lipids in chemical shift imaging on MRI and washout on CT is highly specific for adrenal adenoma; however, clear cell renal cell carcinoma and hepatocellular carcinoma metastases may contain intercellular fat and may show washout on CT scans [19–21]. Other imaging features that favor metastasis over adenoma include increased T2 signal intensity, larger size, heterogeneous

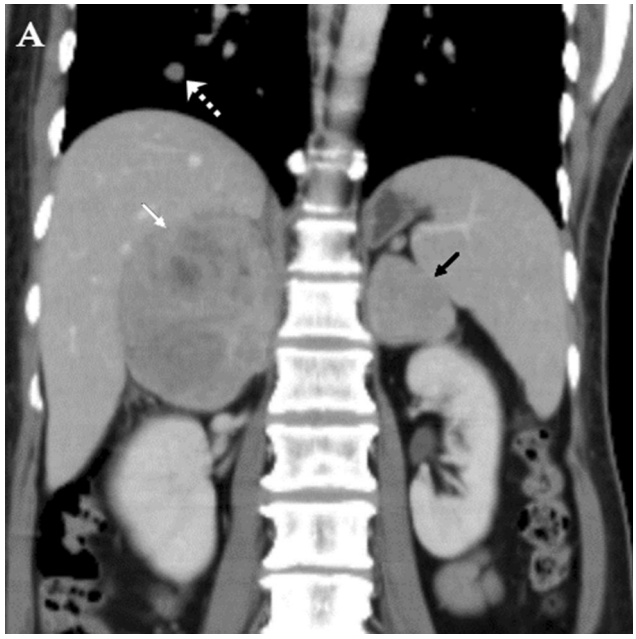

Fig. 5. 60-year-old woman is a known case of melanoma with lung and bilateral adrenal metastases. Coronal contrast-enhanced CT image using soft tissue window shows a heterogeneous large right adrenal masse (white arrow), more homogenous left adrenal lesion (black arrow), and metastatic pulmonary nodule (dashed arrow).

internal texture (Fig. 5), and irregular margins [23, 24]. Diffusion restriction is not very helpful in distinguishing adrenal adenoma from metastasis [25]. Adrenal 18F-fluorodeoxyglucose (FDG) uptake exceeding liver uptake may cause suspicion of malignancy. Most adrenal metastases are FDG-avid; however, some metastases may demonstrate mild uptake (Fig. 6). Moreover, adenomas can show mild FDG uptake. Therefore, mildly FDG-avid lesion in a baseline study for a patient with a history of malignancy should undergo further imaging evaluation or biopsy [26, 27].

Lymphoma

Primary adrenal lymphoma without lymphadenopathy or other extra-nodal disease is rare [28, 29]. Secondary adrenal involvement is seen in about 4% of diffuse non-Hodgkin's lymphoma (NHL), and 43% of these cases are bilateral [30]. About two-thirds of patients with bilateral adrenal involvement had adrenal insufficiency [28].

Adrenal lymphoma tend to grow in an infiltrative manner, maintaining the adreniform appearance. However, it may progress and have heterogeneous enhancement with necrotic or cystic components, which would pose a diagnostic challenge (Fig. 7). On CT, an adrenal lymphomatous mass can be homogeneous with washout features similar to other malignancies. Prior to treatment, calcification is rare. The MR features are non-specific and resemble metastases [29, 31]. Adrenal lymphoma show FDG uptake. After successful therapy, FDG uptake decreases along with other involved sites [32] and the involved adrenal glands usually regress in size and may retain their normal configuration (Fig. 8).

Neuroblastoma

Bilateral neuroblastoma is rare and reported in less than 10% of neuroblastoma cases and in 20% of patients with familial neuroblastoma. Most cases affect patients younger than 6 months with higher incidence of Stage 4S [33, 34]. On CT, neuroblastoma can show homogeneous or heterogeneous internal texture. About 85% of the abdominal neuroblastoma show calcifications on CT scan. Neuroblastoma has a tendency to cross the midline and encase the blood vessels without invasion (Fig. 9) [35].

Pheochromocytoma

Bilateral pheochromocytoma occurs in 10% of the cases. Bilateral pheochromocytomas represent approximately one-third of pathologically examined bilateral adrenal lesions. About two-thirds of bilateral pheochromocytomas are associated with multiple endocrine neoplasia type 2, neurofibromatosis type 1, Von Hippel–Lindau disease, Sturge–Weber syndrome, non-syndromic familial pheochromocytoma, and Carney triad. Functioning pheochromocytoma secretes catecholamines, resulting in palpitations and refractory hypertension [7, 9, 36].

On imaging, pheochromocytoma is known as an imaging "chameleon," because it has variable imaging appearances. It can be homogenous or heterogeneous, can show low attenuation similar to adenoma on non-enhanced CT, and may have areas of cystic degeneration.

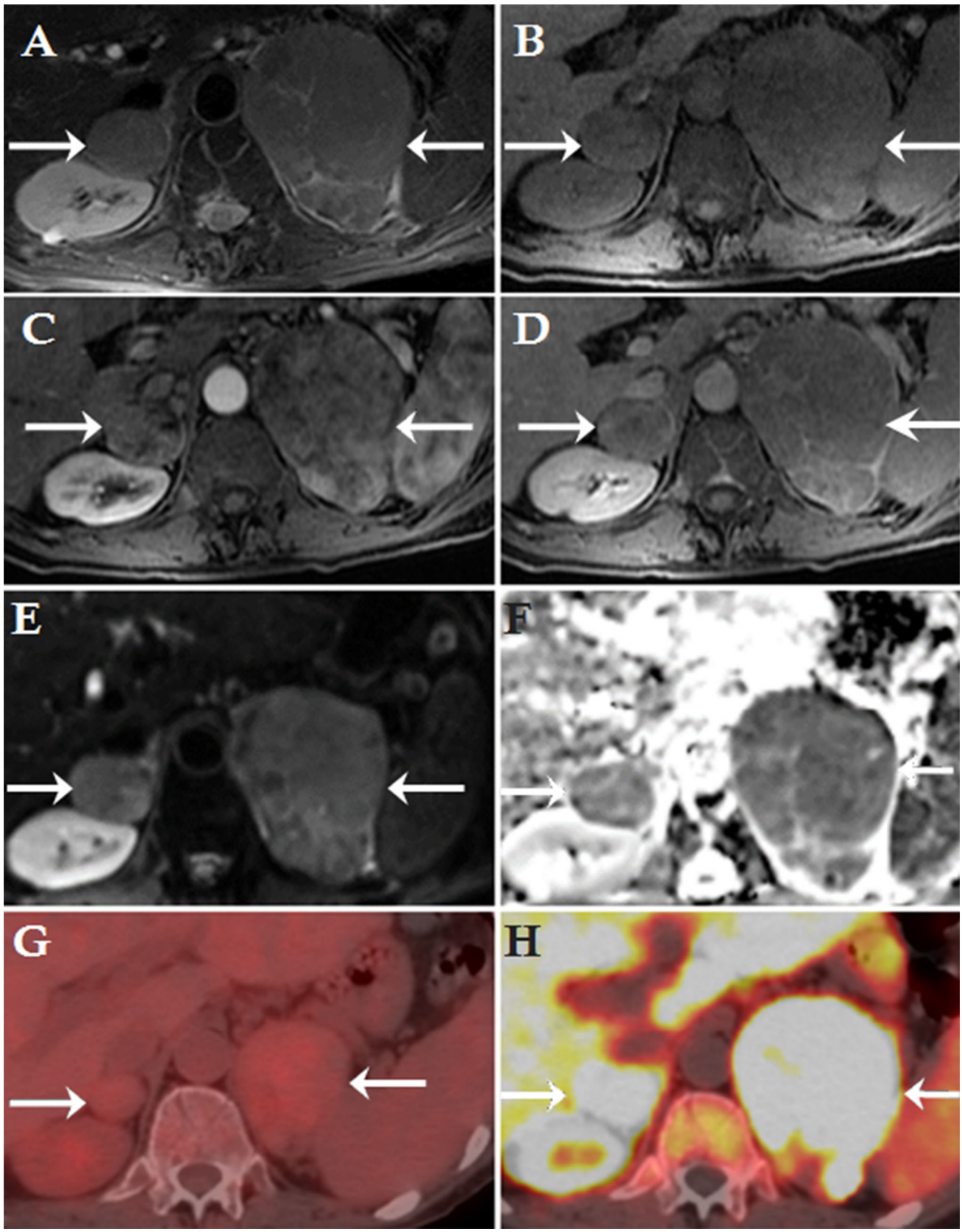
A
B
C
D
E
F
G
H

◀**Fig. 6.** 68-year-old man with bilateral adrenal metastases from hepatocellular carcinoma (HCC). Axial fat-saturated T2-weighted (**A**), pre-contrast T1-weighted (**B**), post-contrast arterial phase (**C**), and delayed post-contrast (**D**) images show bilateral large heterogeneous adrenal masses of intermediately high T2 signal, intermediate T1 signal, and heterogeneous arterial enhancement with washout on the delayed phase. Axial diffusion-weighted (**E**), and apparent-diffusion coefficient (**F**) MRI images show moderate diffusion restriction. Fused axial CT/PET-FDG image (**G**) shows mild heterogeneous FDG uptake (arrows). Fused CT/PET-F18 choline (**H**) image few months after the CT/PET-FDG exam shows interval increase in size and intense F18 choline uptake consistent with HCC metastasis (arrows).

Phaeochromocytoma classically shows intense enhancement, but washout characteristics are variable and may show washout values, similar to adrenal adenoma [37, 38]. The classic MRI appearance of phaeochromocytoma is "light-bulb bright" on T2 weighted images; however, these features are not specific and are not seen in all phaeochromocytomas. About 10% of pheochromocytoma are malignant and show the presence of metastatic disease (Fig. 10) or local invasion, which are reliable signs of malignancy [14, 38, 39]. Metaiodobenzylguanidine (MIBG) has a high sensitivity and specificity for the majority of pheochromocytomas (Fig. 10). MIBG is an analogue of guanethidine and norepinephrine [40].

Myelolipoma

Myelolipoma is a common incidental, hormonally inactive, benign adrenal tumor with no malignant potential. It is bilateral in 5% to 13% of the cases. It contains mainly fatty tissue with scattered haematopoietic elements similar to bone marrow histology. Myelolipoma is

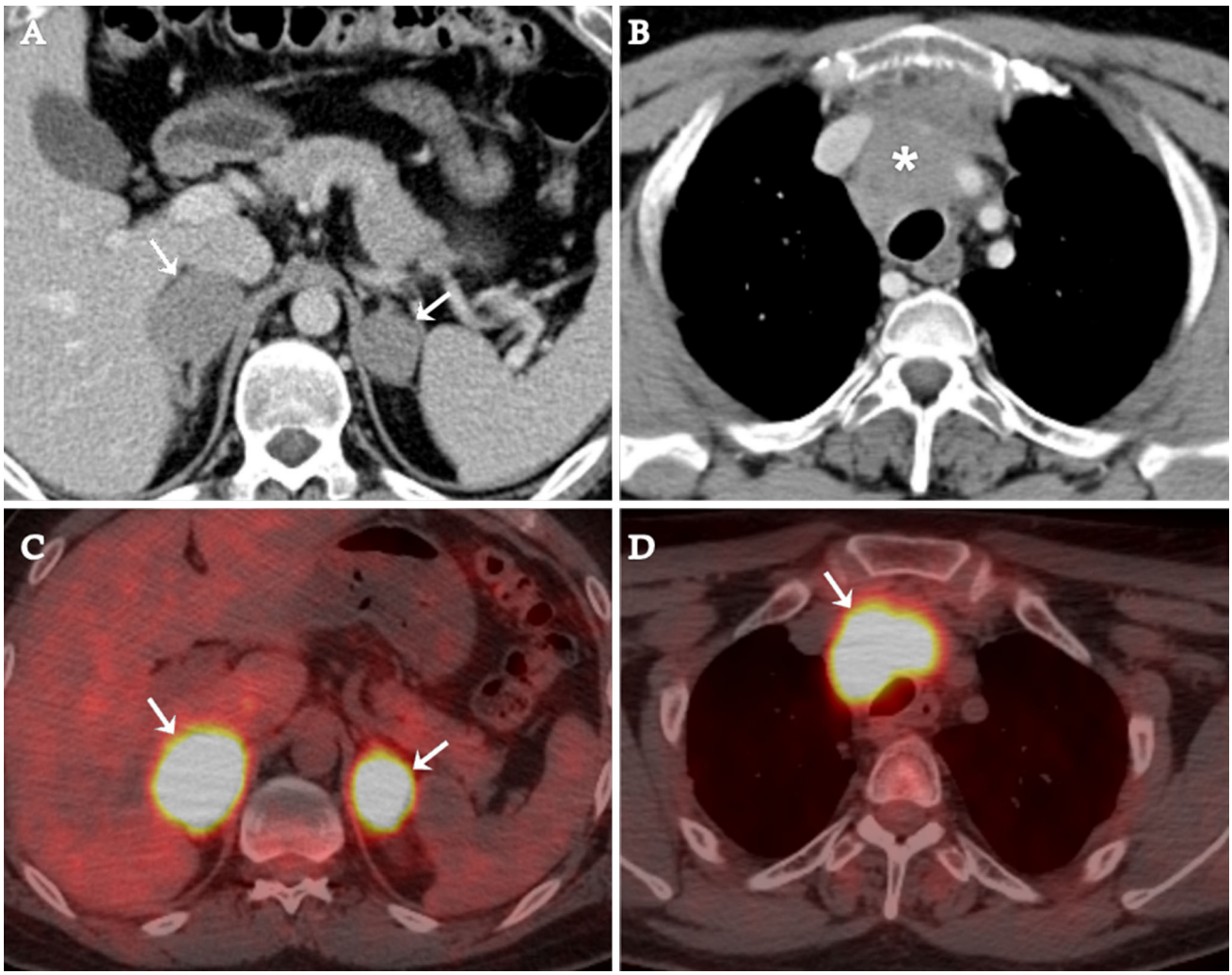

Fig. 7. 27-year-old man with diffuse large B-cell lymphoma. Axial contrast-enhanced CT image (**A**) shows bilateral adrenal homogenous masses (solid arrows). Axial contrast-enhanced CT image (**B**) shows homogenous superior anterior mediastinal soft tissue mass (asterisk). Fused axial CT/PET-FDG images (**C**, **D**) show intense FDG uptake of both adrenals and mediastinal masses (arrows), compatible with lymphoma.

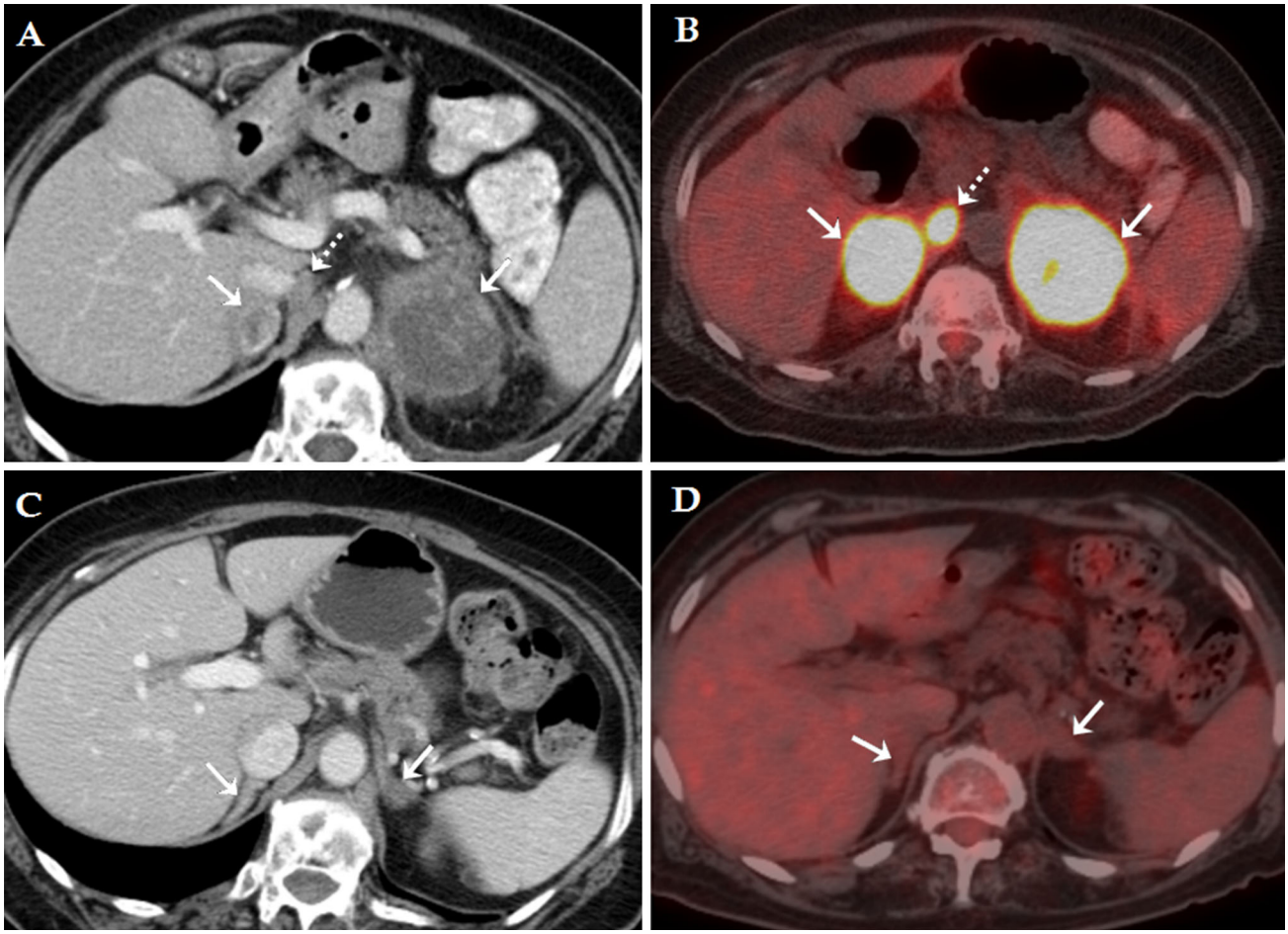

Fig. 8. 64-year-old woman with diffuse large B-cell lymphoma. Axial contrast-enhanced CT (**A**) and fused axial CT/PET-FDG (**B**) images show heterogeneous and FDG-avid bilateral adrenal masses (arrows) with aortocaval lymph node (dashed arrow). Follow-up axial contrast-enhanced CT (**C**) and fused axial CT/PET-FDG (**D**) images after full course of treatment show near complete resolution of the adrenal masses with complete metabolic response (arrows).

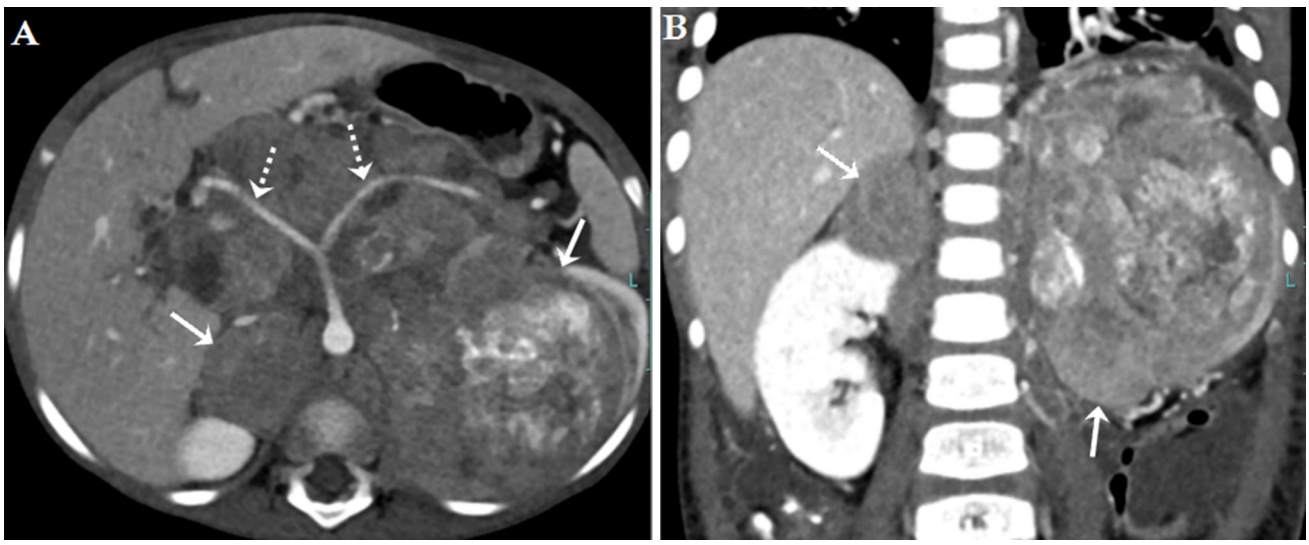

Fig. 9. 4-year-old girl with bilateral neuroblastoma. Axial and coronal contrast-enhanced CT images (**A**, **B**) show bilateral heterogeneous suprarenal masses (arrows). The left suprarenal large mass shows heterogeneous calcifications. The masses cross the midline and encase the blood vessels without invasion (dashed arrows).

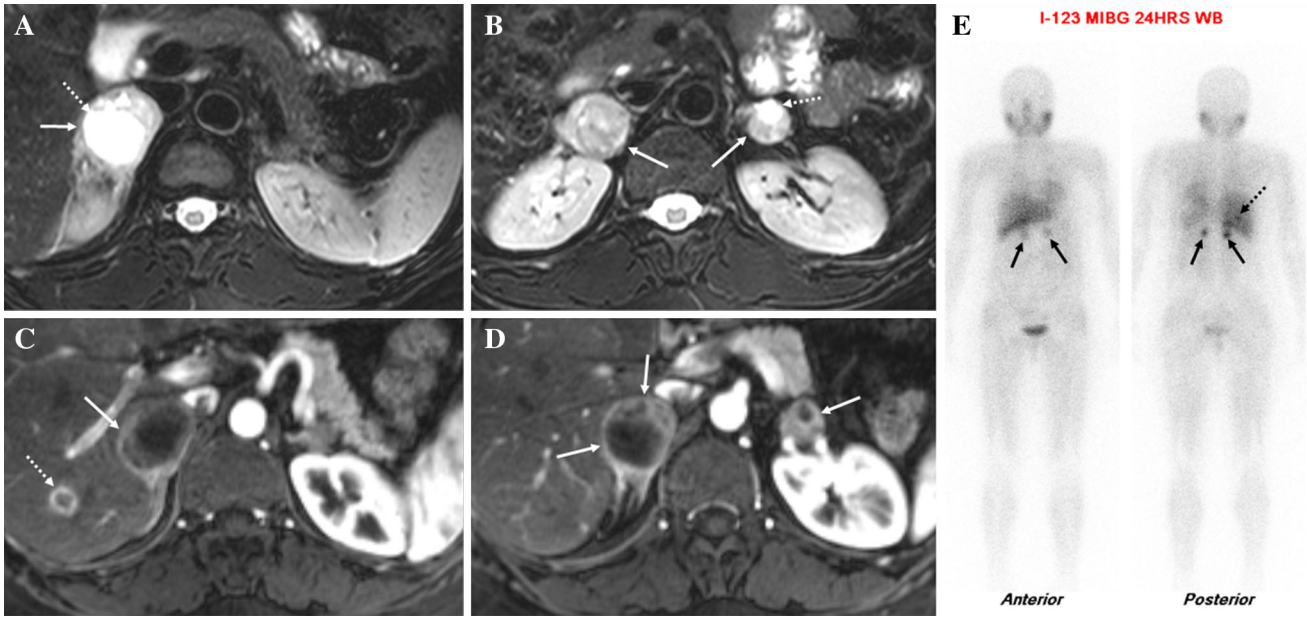

Fig. 10. 47-year-old woman is a known case of type 2 multiple endocrine neoplasia with bilateral pheochromocytomas. Axial fat-T2 weighted MR images (**A**, **B**) show bilateral intermediately high signal adrenal lesions (arrows) with cystic changes (dashed arrows). Arterial (**C**) and delayed (**D**) T1 post-contrast axial MR images show enhancement of the peripheral and solid parts of both adrenal lesions (arrows). Note the hepatic rim-enhancing lesion (dashed arrow), consistent with a metastatic lesion. Iodine-123 MIBG study (**E**) shows intense uptake of both adrenal lesions (arrows) and the metastatic liver lesion (dashed arrow).

usually asymptomatic, unless it is large, resulting in a mass effect or, rarely, complicated by bleeding [14, 41]. Congenital adrenal hyperplasia (CAH) may be associated with adrenal myelolipomas, usually unilateral but some are bilateral. It is assumed that prolonged exposure to elevated ACTH levels plays a role in the development of adrenal myelolipoma in patients [9, 42].

On imaging, the presence of macroscopic fat is the main diagnostic feature. On CT, the lesion contains macroscopic fat (HU < -30) with interspersed soft tissue attenuation myeloid tissue (Figs. 11 and 12). Macroscopic fat on MRI shows high signal intensity on both T1 and T2 weighted images, which suppresses with frequency selective fat saturation. Exophytic renal angiomyolipoma and retroperitoneal fat-containing lesion may occupy the suprarenal region mimicking adrenal myelolipoma. Therefore, careful evaluation and determination of the lesion origin using different imaging planes is essential [14]. Macroscopic fat is not exclusively specific for adrenal myelolipoma. Differential considerations of adrenal lesion with macroscopic fat are not limited to myelolipoma and include adenoma with myelo-lipomatous degeneration and adrenal cortical carcinoma [43, 44]. However, some authors suggest that any fat-containing adrenal lesion and macroscopic fat representing more than 50% of lesion should be managed as myelolipoma [45]. The fat represented more than 50% of about 80% of radiologically and pathologically evaluated myelolipomas [43]. The presences of irregular margins, heterogeneity, and local invasion should raise the possibility of rare fat-containing malignancy.

Infectious adrenal process

Tuberculosis is one of the most common infectious organisms affecting adrenal glands. The incidence of adrenal tuberculosis is declining in the developed countries, but is still a common cause of bilateral adrenal

Fig. 11. 67-year-old patient with incidental bilateral myelolipoma. Coronal contrast-enhanced CT image (**A**) and two axial images (**B**, **C**) show bilateral adrenal lesions containing macroscopic fat (arrows), consistent with bilateral adrenal myelolipomas.

lesions and adrenal insufficiency in developing countries. Adrenal tuberculosis can result in progressive glandular destruction, which may eventually lead to adrenal insufficiency. The symptoms of adrenal insufficiency are usually non-specific and insidious, including weakness, fatigue, nausea, anorexia, and vomiting [7, 9, 46].

Both adrenal glands are affected in the majority of the cases [7, 9, 46, 47]. At the early stage, CT examination frequently shows adrenal mass-like enlargement. Also, enlarged adrenal glands with preserved contour are a suggestive feature of infectious etiology, as compared with most of tumors, which commonly show round or

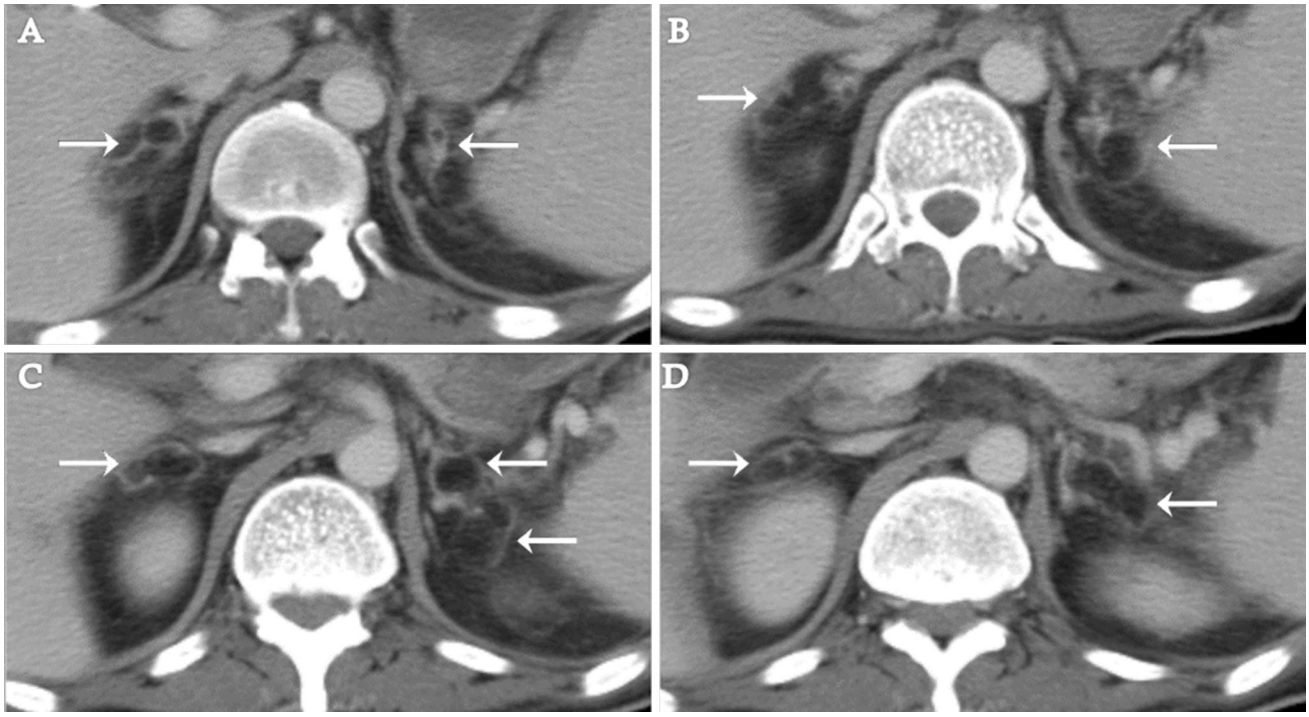

Fig. 12. Incidentally detected multiple bilateral adrenal myelolipomas. Multiple axial contrast-enhanced CT images (**A**–**D**) show multiple bilateral adrenal fatty lesions replacing most of the adrenal glands (arrows), compatible with multiple bilateral adrenal myelolipomas.

oval adrenal masses [46–49]. Adrenal enlargement with central low attenuation and a peripherally enhancing rim is another suggestive feature of adrenal tuberculosis (Fig. 13). At an advanced stage, the enlarged adrenal glands regress in size or may retain normal size and configuration due to fibrosis and calcification. Although calcifications can be seen during different stages of adrenal tuberculosis, their prevalence is higher in chronic cases [46–48]. The presence of atrophied adrenals with calcification is highly suggestive of adrenal tuberculosis [50]. Adrenal lesion with calcification is not typical in primary adrenal malignancy, metastasis and untreated lymphoma [46, 49].

Imaging features suggestive of extra-adrenal tuberculosis involving lungs, lymph nodes, peritoneum, and the spine are helpful, but non-specific, clues in the diagnosis of adrenal tuberculosis. However, about 12% of patients with adrenal tuberculosis may not have evidence of extra-adrenal tuberculosis [51]. Also, other infectious processes such as adrenal histoplasmosis can mimic tuberculosis [52], adrenal lymphoma and metastasis, but in the differential diagnosis of bilateral heterogeneous adrenal lesions. Therefore, adrenal biopsy is appropriate in such clinical settings to confirm diagnosis and commence anti-tuberculosis drugs.

Haematoma

Adrenal hemorrhage is caused by trauma and other non-traumatic etiologies. Bilaterality is seen in about 20% of cases. Non-traumatic etiologies include coagulopathy, stress, venous hypertension, and hemorrhagic tumor.

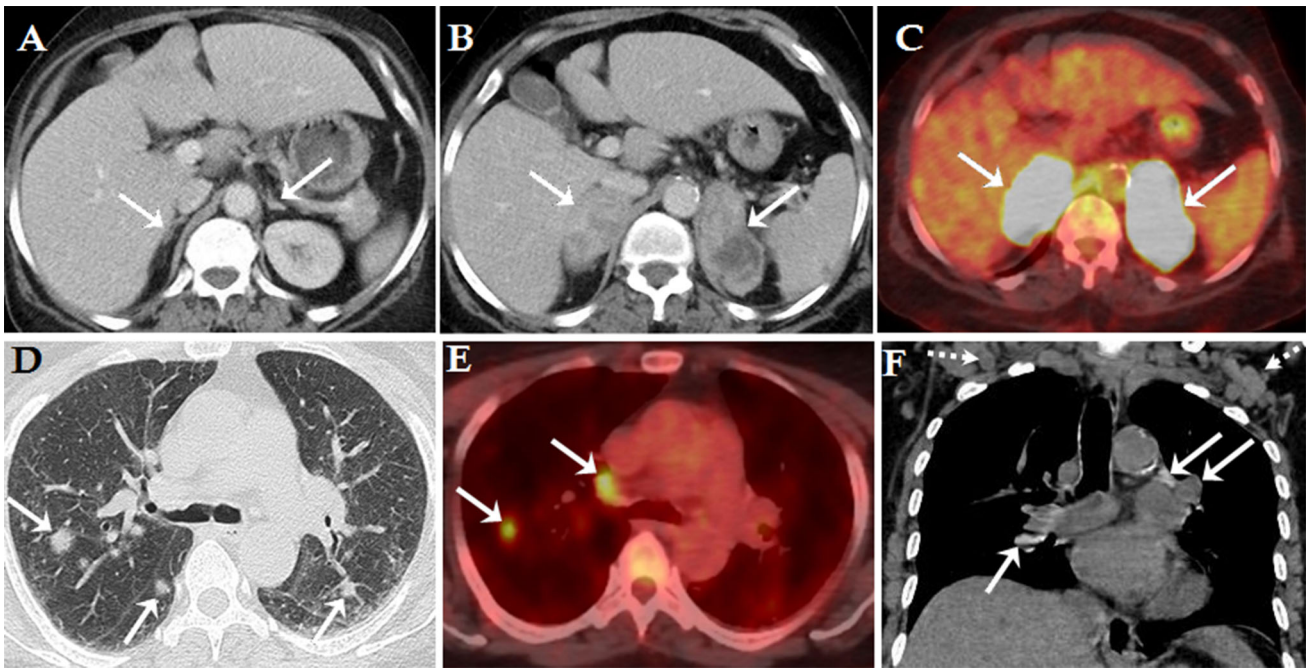

Fig. 13. 70-year-old woman, known case of treated lymphoma (classical Hodgkin's lymphoma), presented with abdominal pain. Axial contrast-enhanced CT image (**A**) few years prior to the current acute presentation shows normal adrenal glands (arrows). Axial contrast-enhanced CT (**B**) and corresponding fused axial CT/PET FDG (**C**) images, at time of current acute presentation, show new bilateral heterogeneously enhancing and FDG-avid adrenals masses (arrows). Non-enhanced axial chest CT image using lung window (**D**) shows multiple lung nodules (arrows). Fused axial CT/PET FDG image (**E**) shows FDG-avid lung nodule and mediastinal lymph node. Coronal chest CT image using soft tissue window (**F**) shows calcified and non-calcified mediastinal and hilar lymph nodes (arrows), and bilateral supraclavicular lymph nodes, some of them are showing central low attenuation (dashed arrows). Imaging features and history of lymphoma were highly suggestive of relapsed disease; however, adrenal and lung biopsies revealed disseminated tuberculosis.

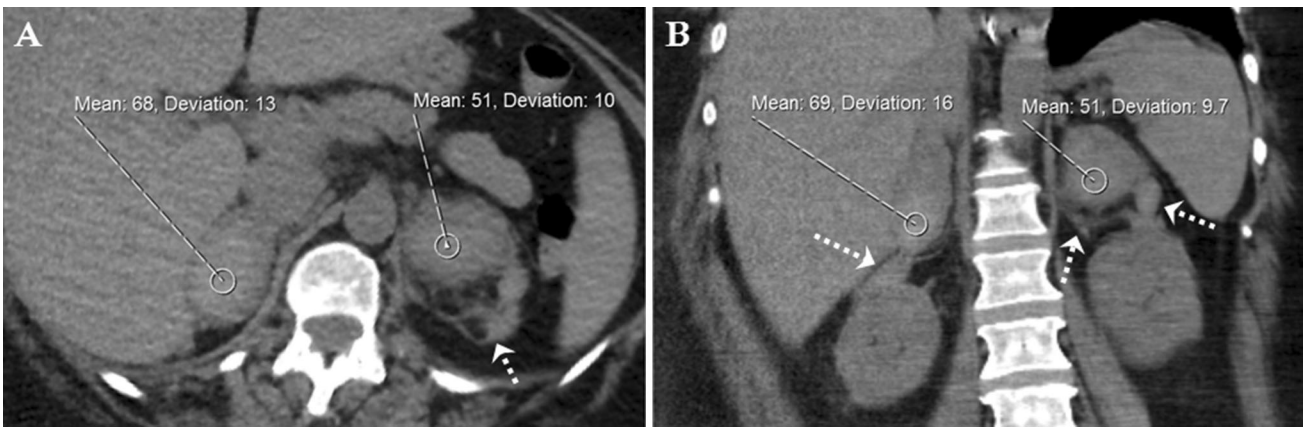

Fig. 14. 51-year-old man with septic shock, on anticoagulant. Axial and coronal non-enhanced CT images (**A**, B) show bilateral adrenal enlargement with relatively homogenous high attenuation (right adrenal HU = 68 and left adrenal HU = 51), consistent with adrenal hemorrhage. Note the surrounding high attenuation component (blood) and fat stranding (dashed arrows).

Stress causes that may result in adrenal hemorrhage include sepsis, hypotension, and surgery. The clinical manifestations are variable and may present with upper abdominal, back or flank pain with possibly signs of blood loss. Bilateral adrenal hemorrhage is a rare cause of Addison's disease [53–55].

On non-enhanced CT, acute and subacute adrenal haematoma appear as hyperattenuating (50–90 HU) adrenal mass with peri-adrenal fat stranding and possible extension into the perinephric space (Fig. 14). Over time, haematoma shows reduction in size and attenuation values, and usually resolves completely. Other possible long-term outcomes of adrenal hemorrhage include calcifications and pseudocyst formation. On MRI, hematoma in the acute stage (< 7 days) shows isointensity to mild hypointensity on T1-weighted sequence, and remarkable hypointensity on T2-weighted sequence. During the subacute stage (1–7 weeks), haematomas show hyperintensity on both T1-weighted and T2-weighted sequences. Blood products of different stages will result in heterogeneous signal (Fig. 15). Classically, there is a dark rim on both T1 and T2 sequences during the chronic stage (>7 weeks) secondary to hemosiderin deposition [53–55].

In patients presenting with non-traumatic adrenal hemorrhage without risk factors, it is essential to exclude any underlying hemorrhagic neoplasm or venous congestion. Adrenal congestion can be caused by adrenal vein, renal vein, or IVC thrombosis. Adrenal congestion can be suggested by adrenal thickening and surrounding fat stranding [56]. Contrast-enhanced CT or MRI is helpful to assess for any venous thrombosis or any enhancing solid component using a subtraction technique. Follow-up imaging is also helpful to ensure interval reduction in size and to rule out an underlying tumor.

Miscellaneous lesions

Adrenal haemangioma is rare and bilaterality of such an entity is even rarer. Adrenal haemangioma is usually cavernous and encapsulated. They have rich peripheral vascularity and complex central components secondary to necrosis, calcification, fibrosis, thrombosis, and hemorrhage. CT scans usually show calcifications and may clearly show phleboliths. They tend to have peripheral enhancement. Centripetal enhancement is less common as compared to liver haemangiomas because of the higher tendency of central necrosis in adrenal haemangiomas. On MRI, adrenal haemangioma shows heterogeneously low signal intensity on T1-weighted MR images and bright signal intensity on T2-weighted images except in the central fibrotic areas, and the enhancement pattern is similar to CT. Adrenal haemangioma may show cystic changes with peripheral and septal enhancement [45, 57]. Adrenal haemangioma usually poses a diagnostic challenge due to their rarity, lack of specific imaging features, and central necrosis and large size mimicking malignant lesion. In such cases, surgical consultation and consideration of resection is usually appropriate.

In this pictorial review, we have presented a rare and unusual case of bilateral adrenal involvement in a patient with Klippel–Trenaunay syndrome (Fig. 16). The differential consideration of bilateral predominately cystic adrenal lesions with scattered calcifications and peripheral and septal enhancement in this patient is suggestive of thrombosed and organized haemangioma or venolymphatic malformation. Klippel–Trenaunay syndrome with unilateral adrenal involvement was previously reported [58, 59].

Diffuse bilateral adrenal processes

Enlargement

Adrenal hyperplasia is a non-malignant growth and enlargement of the adrenal glands parenchyma. Generally, normal adrenal limb thickness is less than 5 mm. The normal shape of adrenal glands is variable and could have inverted V, inverted Y, triangular, or linear configuration. Adrenal hyperplasia can be congenital or acquired, smooth or nodular, and adrenocorticotropic

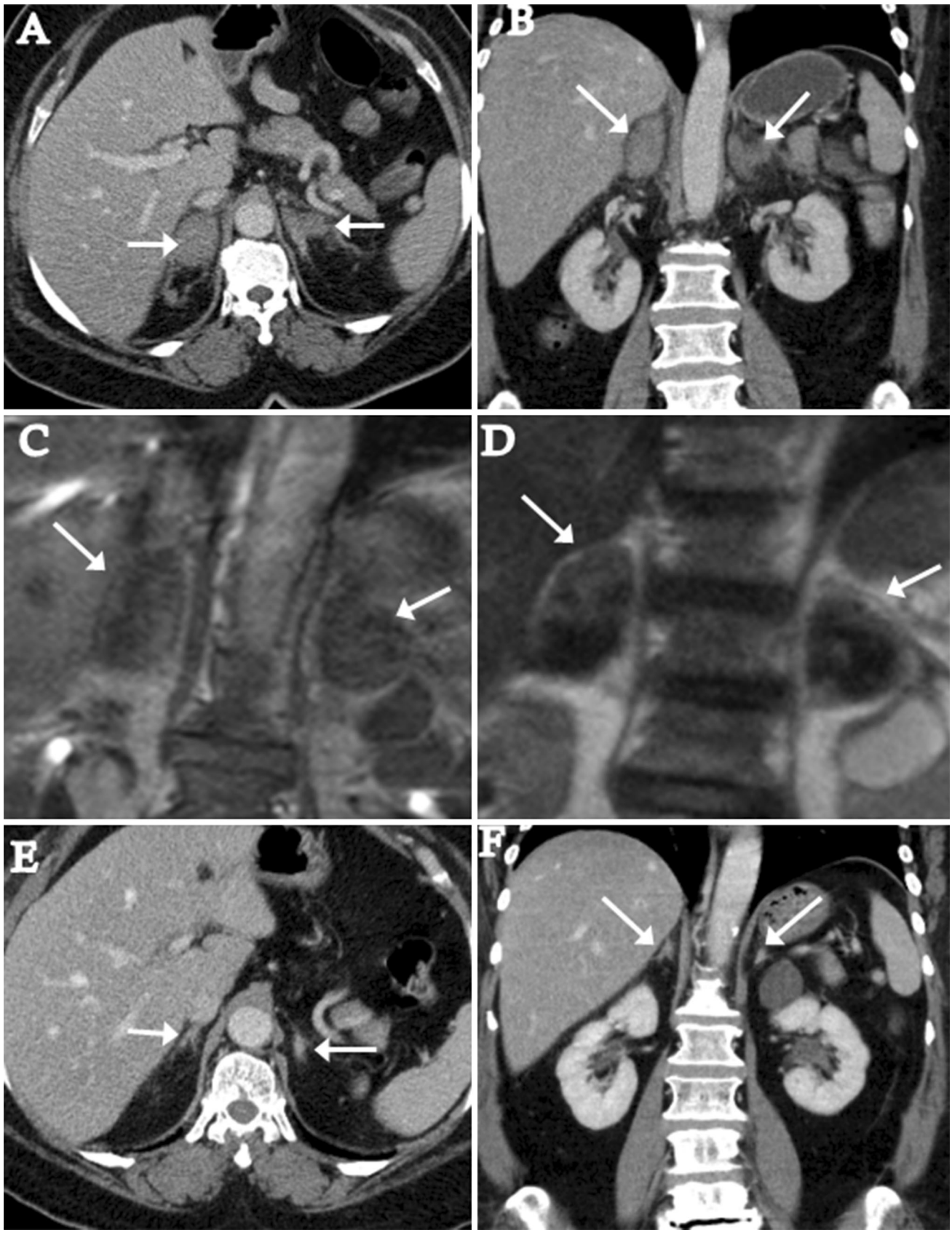
A
B
C
D
E
F

◀**Fig. 15.** 74-year-old woman post total knee replacement on anticoagulant, complaining of abdominal pain. Axial and coronal contrast-enhanced CT images (**A**, **B**) show bilateral adrenal enlargement with increased attenuation and surrounding fat stranding. Coronal T1-weighted (**C**) and T2-weighted (**D**) MR images show bilateral adrenal enlargement with heterogeneous and predominantly central low signal intensity with peripheral foci of intermediately high signal intensity (arrows). Axial and coronal contrast-enhanced CT images (**E**, **F**) after 8 months show interval resolution of both hematomas (arrows).

hormone (ACTH)-dependent or ACTH-independent [60–64].

Hypercortisolism in ACTH-dependent cases derive from pituitary origins (Cushing's disease) or other non-pituitary sources such as administration of exogenous glucocorticoids or ectopic ACTH-secreting tumor (Cushing's syndrome). ACTH-dependent adrenal hyperplasia are commonly smooth (Fig. 17) or lobular, and less commonly nodular. In the case of Conn's syndrome (hyperaldosteronism), with no imaging evidence of adrenal adenoma, adrenal hyperplasia is suspected as an underlying etiology [61, 62].

ACTH-independent hypercortisolism represents 15% to 20% of Cushing syndrome cases, and is commonly due to functioning adrenal adenoma or carcinoma. Other rare causes of ACTH-independent Cushing syndrome include primary pigmented nodular adrenal dysplasia (PPNAD) and ACTH-independent macronodular adrenal hyperplasia (AIMAH). The PPNAD is known as bilateral micronodular adenomatosis and micronodular adrenal disease. The PPNAD can be isolated or associated with Carney complex. On imaging, adrenal glands may be normal or mildly enlarged with multiple small nodules. On the other hand, the AIMAH characteristically shows remarkably enlarged adrenal glands with multiple large nodules and masses. The AIMAH may show signal drop on OP images indicative of intracellular fat and confusion with multiple adrenal adenomas (Fig. 18). The treatment of choice for these two rare entities is bilateral adrenalectomy and glucocorticoid replacement [63–65].

In CAH, one of the enzymatic steps, most commonly 21-hydroxylase enzyme, required to form cortisol from cholesterol, is deficient. This results in different degrees of mineralocorticoid and cortisol deficiency. The interruption of negative feedback inhibition of ACTH by the pituitary gland results in adrenal cortical hyperplasia. On imaging, adrenal glands show enlargement (Fig. 19) with preserved adrenal configuration [64]. The CAH can be associated with adrenal myelolipoma [9, 42].

Not every adrenal enlargement is attributed to adrenal hyperplasia. Other pathological entities may present on imaging mainly as adrenal enlargement, such as adrenal metastasis, lymphoma [14], infectious processes such as tuberculosis [46], adrenal congestion [56], inflammatory processes such as Rosai–Dorfman disease [8], and other systemic conditions such as neurofibromatosis type-1[64].

Atrophy

Adrenal insufficiency is due to inadequate release of corticosteroids. Primary adrenal insufficiency is also known as Addison's disease. Secondary adrenal insufficiency is due to lack of stimulation of the adrenal gland by the pituitary gland. Adrenal insufficiency is a clinical and laboratory diagnosis. The most common cause of Addison's disease is idiopathic autoimmune disorders. Granulomatous disease, such as tuberculosis, is the most common cause in developing countries. Other causes include sarcoidosis, bilateral adrenal hemorrhage, bilateral neoplasms such as metastases and lymphoma [50, 60].

Imaging features depend on the cause and the course of the disease. During the chronic stage, both adrenals appear atrophic and small (Fig. 20). Associating adrenal calcifications (Fig. 21) is highly suggestive of prior granulomatous adrenalitis [60, 66]. Adrenal insufficiency could also be present on imaging with adrenal enlargement, in the case of bilateral infectious process or adrenal malignancy [48].

Calcifications

Wolman's disease is a rare autosomal recessive inborn error of metabolism resulting in fat deposition in multiple organs, including the liver, spleen, and lymph nodes. Patients usually present during the first few months of life, with diarrhea, vomiting, and failure to thrive. Treatment of Wolman's disease is primarily supportive and generally carries a poor prognosis [67].

On imaging, both adrenal glands are enlarged and calcified. The diffuse adrenal enlargement with predominantly peripheral calcification is due to cholesterol and fatty acid crystal deposition and saponification within the adrenal cortex. On MRI, the calcifications show low signal intensity on all sequences. CT may show hepatosplenomegaly, with diffuse liver low attenuation due to fatty infiltration (Fig. 22). Also, low attenuation lymphadenopathy can be seen [68, 69].

Intense enhancement: hypoperfusion complex

In unwell patients with hypoperfusion status, the adrenal glands demonstrate symmetric bilateral intense enhancement with attenuation values matching the great vessels such as abdominal aorta or inferior vena cava (IVC). IVC slit-like flattening, increased renal enhancement and diffuse bowel wall thickening are another supportive diagnostic imaging clues of hypoperfusion complex (Fig. 23). This phenomenon is related to a sympathetic response to shock to preserve the perfusion of vital organs including the adrenals [70].

Fig. 16. 32-year-old woman is a known case of Klippel-Trenaunay syndrome. Coronal contrast-enhanced CT (**A**), and coronal T2-weighted (**B**), pre-contrast T1-weighted (**C**), and post-contrast T1-weighted (**D**) images show a predominantly cystic bilateral adrenal lesions with peripheral and septal enhancement (white arrows) and few calcifications (black arrows). The adrenal lesions show high signal foci in the pre-contrast T1 weighted images (dashed arrows) with no corresponding enhancement, differential considerations include blood product or proteinaceous fluid. The enlarged heterogeneous spleen (white asterisk), retroperitoneal insinuating cystic lesion (black asterisk, likely lymphangioma), and left thigh subcutaneous and muscles heterogeneous attenuation (image **A**) are related to the disease involvement.

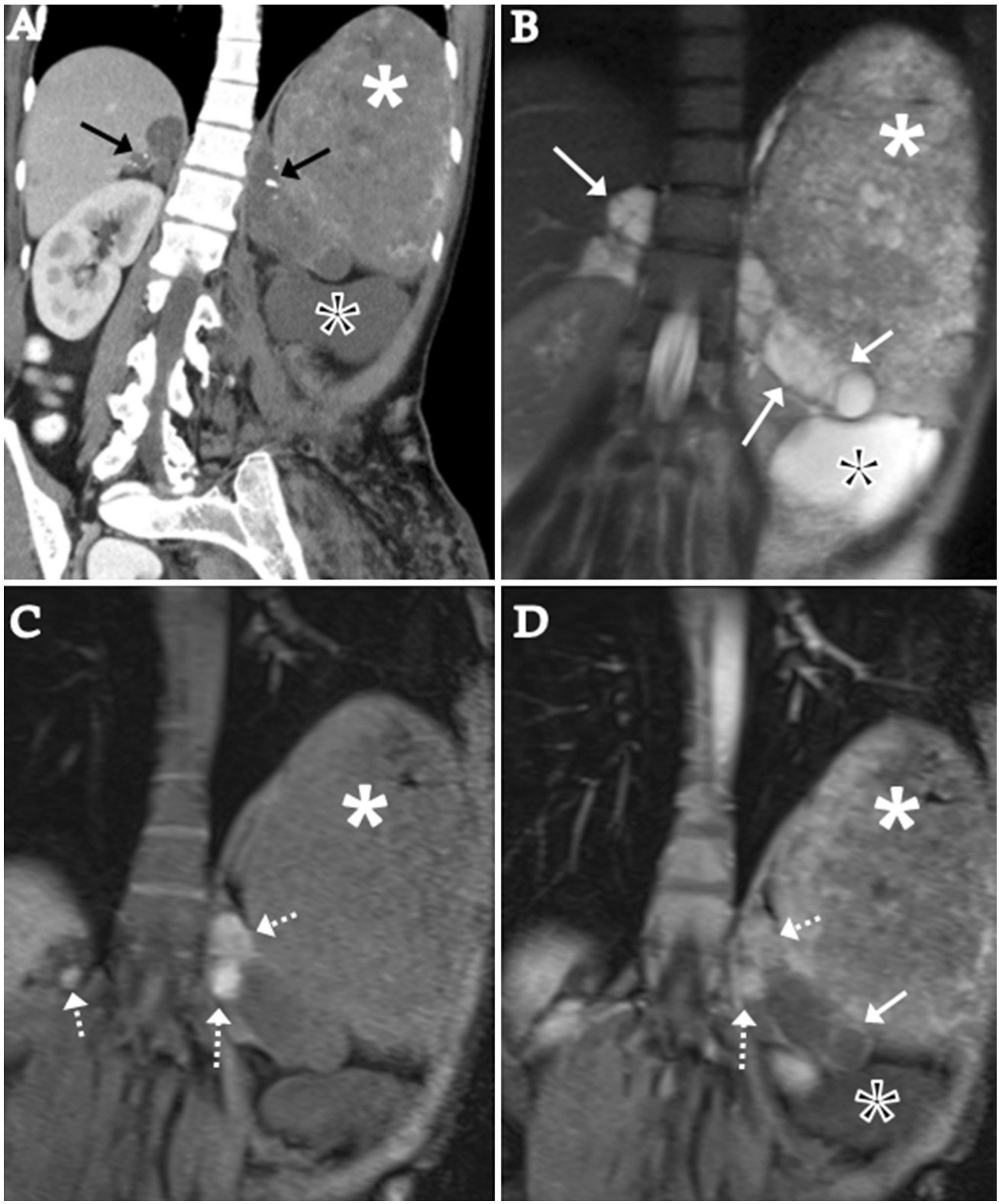
A
B
C
D

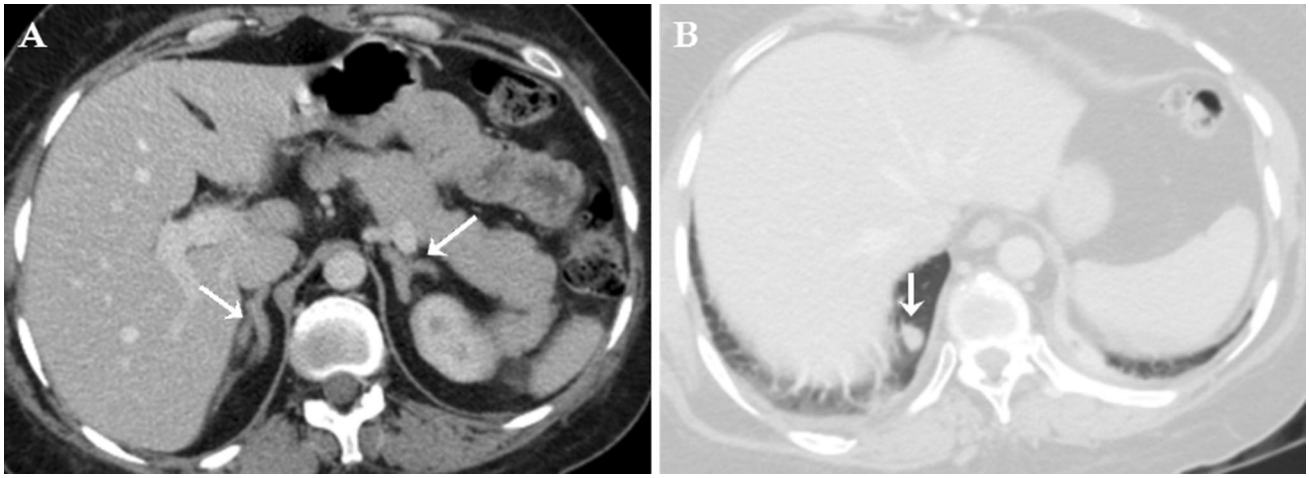

Fig. 17. 37-year-old woman with Cushing syndrome. Axial CT image at portal venous phase (**A**) shows smooth bilateral adrenal enlargement with preservation of the adreniform shape (arrows). Axial CT image utilizing lung window at the level of lung bases (**B**) shows right lower lobe 9-mm nodule (arrow). Resection and histopathological assessment of this lung nodule revealed a carcinoid tumor. The overall findings are indicative of ACTH-dependent Cushing syndrome due to ectopic ACTH source from lung carcinoid tumor.

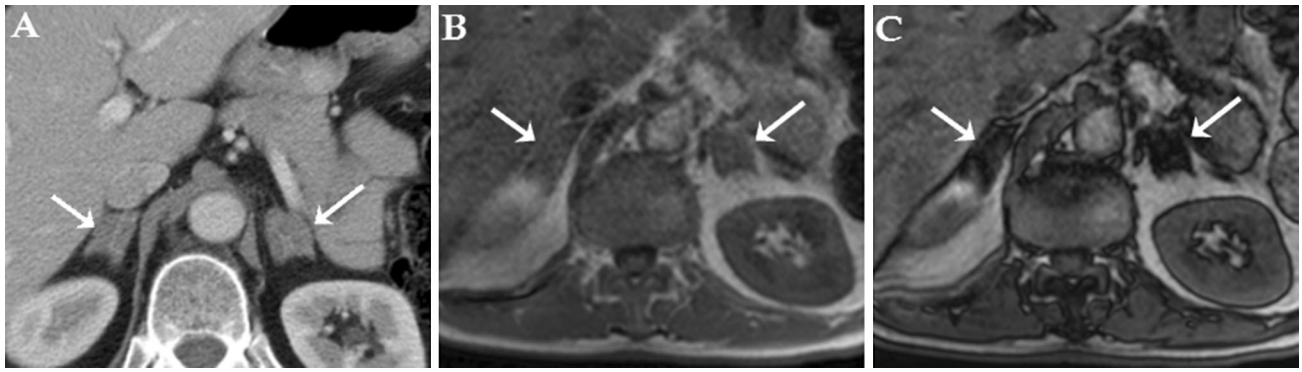

Fig. 18. 56-year-old man is a known case of rectal cancer with incidental findings suggestive of adrenal hyperplasia. Axial contrast-enhanced CT image (**A**) shows bilateral adrenal thickening with relative preservation of the adreniform shape (arrows). Axial in-phase T1 weighted MR image (**B**) shows intermediate signal intensity of both adrenal glands (arrows). Axial out-phase T1 weighted MR image (**C**) shows diffuse signal drop of both adrenal glands (arrows), consistent with intracellular fat.

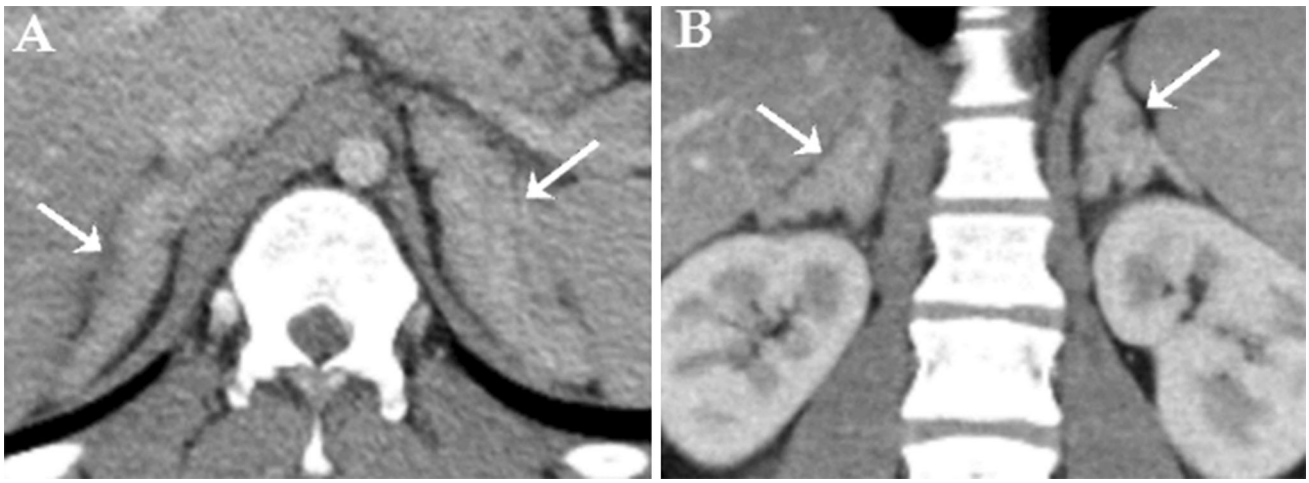

Fig. 19. 16-year-old boy with congenital adrenal hyperplasia. Axial (**A**) and coronal (**B**) contrast-enhanced CT images show bilateral adrenal diffuse nodular enlargement with preservation of the adreniform shape (arrows).

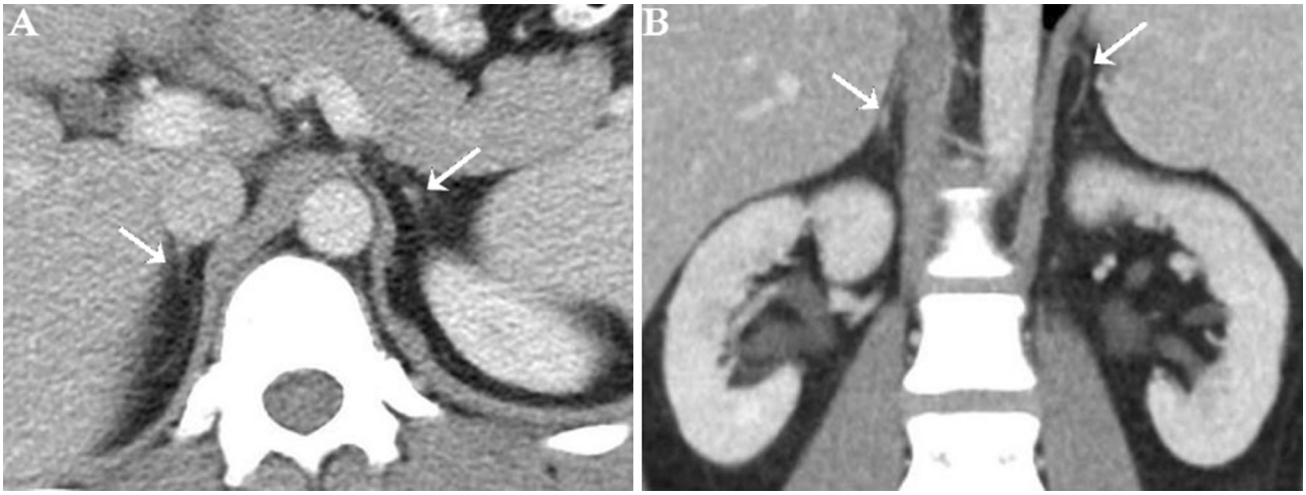

Fig. 20. 32-year-old man is a known case of primary Addison's disease for years. Axial and coronal contrast-enhanced CT images show remarkably small atrophic adrenal glands (arrows) with no adrenal calcifications.

Infarction

Adrenal infraction is rare, due to the rich blood supply of the adrenal glands. The arterial supply of the adrenal gland arises from the inferior phrenic artery, directly from the aorta, and from the renal artery. There is a single draining adrenal vein on each side. It is suggested that microvascular and venous thrombosis in hypercoagulable states can lead to adrenal infarction. Adrenal infarction commonly associated with hemorrhage. However, adrenal infarctions without hemorrhage were reported. On imaging, those cases showed adrenal enlargement with no MRI signs of blood product, or adrenal enlargement with normal attenuation on non-enhanced CT or with no adrenal parenchymal enhancement on enhanced CT (Fig. 24). Therefore, adrenal infarction should be considered in the differential diagnosis in patients with abdominal pain, underlying hypercoagulable state and enlarged adrenals on imaging. Bilateral adrenal infarctions may result in adrenal insufficiency [71–74].

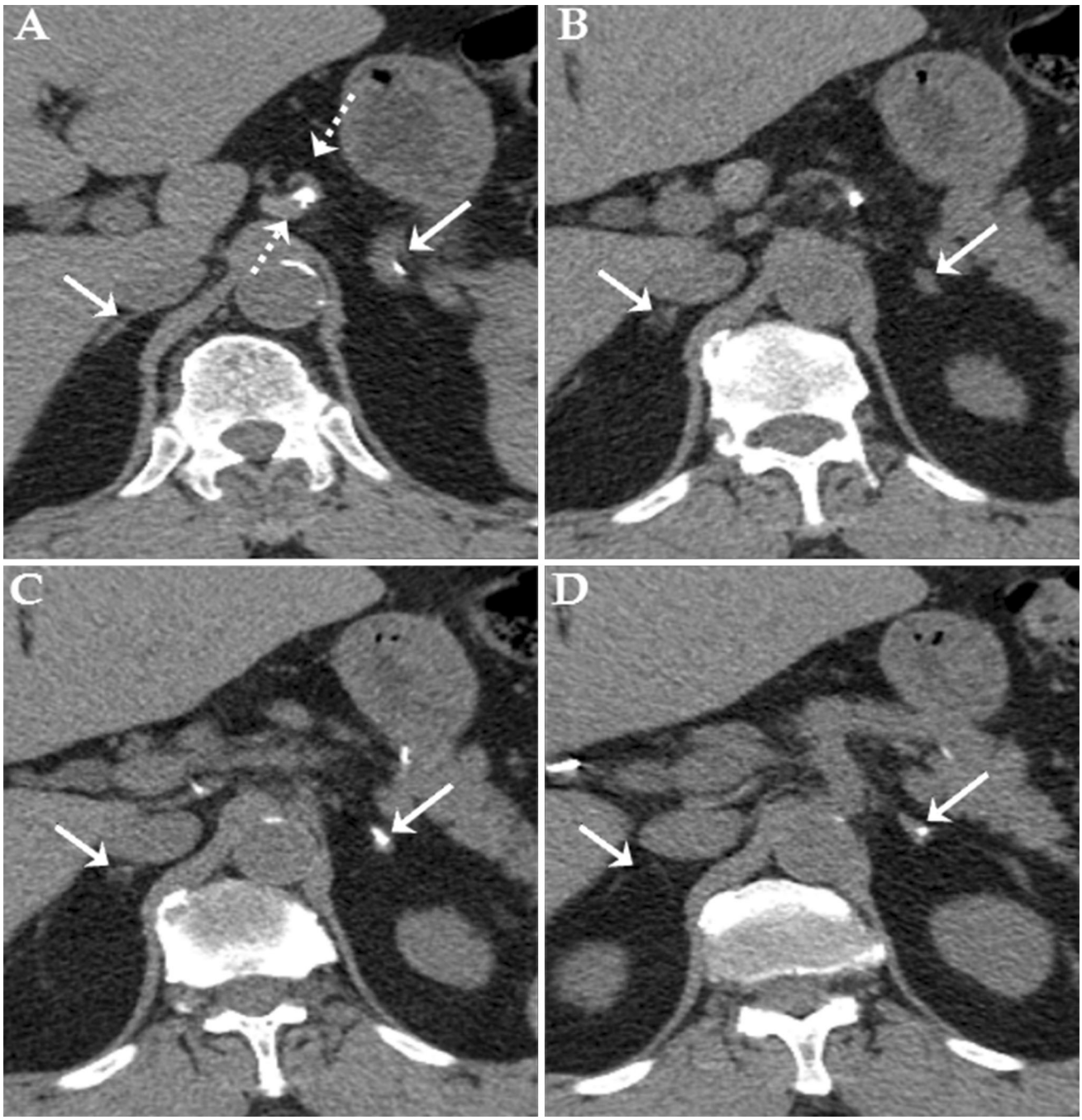

Fig. 21. 79-year-old man is a known case of primary Addison's disease. Multiple axial contrast-enhanced CT images (**A**–**D**) show small right adrenal gland and partially calcified left adrenal gland (solid arrows). There is a calcified retroperitoneal lymph node (dashed arrow). The presence of calcified lymph node and left adrenal calcifications is suggestive of prior granulomatous disease such as tuberculosis.

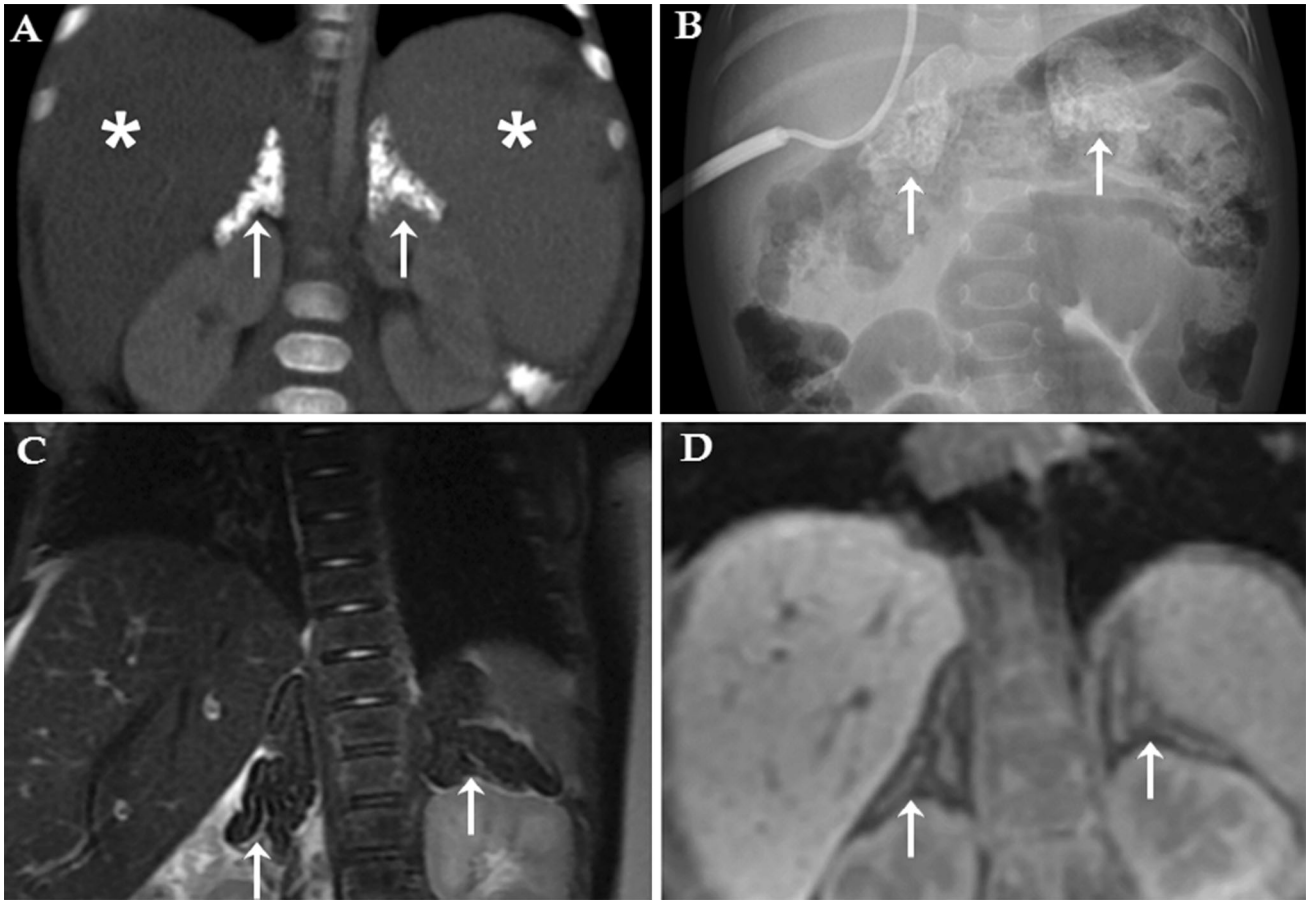

Fig. 22. 3-month-old male infant is a known case of Wolman's disease. Coronal CT image (**A**) shows diffuse bilateral adrenal enlargement and calcification with preservation of the adreniform shape (arrows). Note the hepatosplenomegaly with diffuse liver low attenuation suggestive of fatty infiltration (asterisks). Frontal abdominal radiograph (**B**) of another 11-month-old infant with Wolman's disease shows bilateral enlarged calcified adrenal glands with preservation of the adreniform shape (arrows). Coronal fat-suppressed T2 weighted image (**C**) and T1-weighted (**D**) images of the same patient in image (**B**) show bilateral adrenal enlargement and peripheral low signal rim representing calcification (arrows).

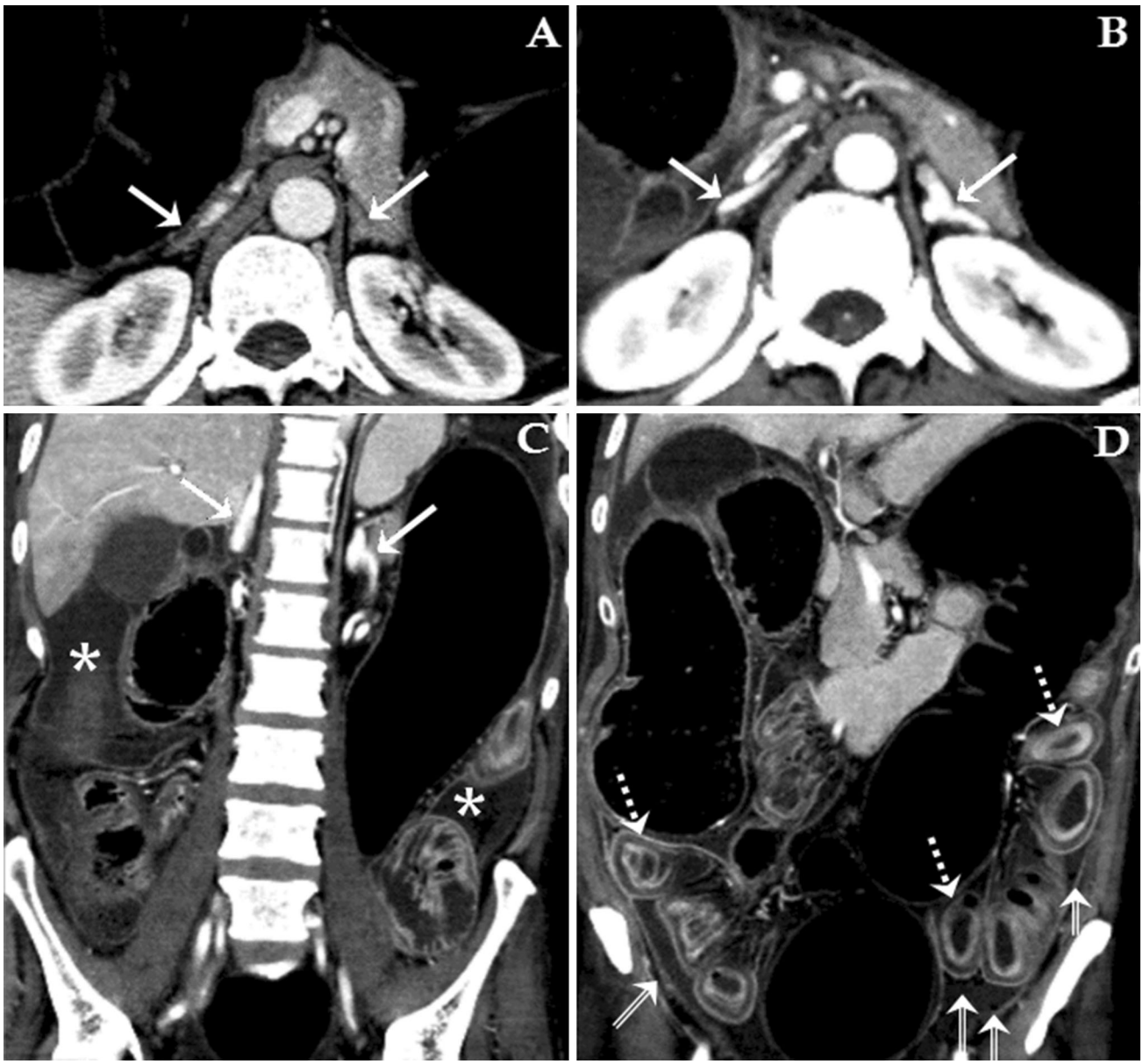

Fig. 23. 58-year-old man is a known case of rectal cancer complicated by perforation and shock. Axial contrast-enhanced CT image few days prior to the acute presentation (**A**) shows normal size and enhancement of both adrenals. Axial and coronal contrast-enhanced CT images (**B**–**D**) show interval mild bilateral adrenal enlargement with intensely enhancement (solid arrows), matching the great vessels attenuation. There is diffuse small bowel wall thickening with inner wall hyperenhancement (dashed arrows), free fluid (asterisks), foci of free air and enhancing peritoneal lining (arrows with double line). These findings are compatible with hypoperfusion complex due to perforated viscus.

Fig. 24. 44-year-old woman is a known case of anti-phospholipid syndrome presented with bilateral adrenal infarctions. Multiple axial contrast-enhanced CT images (**A**–**D**) show bilateral mildly enlarged adrenals with diffuse reduced enhancement of most the adrenal glands and surrounding fat stranding (arrows). There is sharp demarcation between the distal parts with preserved enhancement and the more proximally less enhancing glands (dashed arrows). Axial contrast-enhanced CT image (**E**) few months prior to the adrenal infarction shows normal adrenals (arrows). Axial contrast-enhanced CT image (**F**) few years after the infarction at the same level in image (**E**) shows interval reduction in size of both adrenal glands suggestive of adrenal atrophy (arrows).

Table 1. The differential diagnosis and imaging features of bilateral adrenal masses [10, 14, 15]

Entity	Bilaterality (%)	NECT	CECT	CS-MRI	Other features
Adenoma	20	HU < 10 is diagnostic for 70% of adenomas (lipid rich)	APW > 60% and ARW > 40% are highly specific for both lipid-rich and lipid-poor adenomas	Signal drop of in opposed-phase. Characterize lipid-rich adenoma and some of the lipid-poor adenomas	Typical adenoma is small (< 4 cm), well defined, and homogenous. Atypical adenoma may be large and heterogeneous with hemorrhage, calcifications, or cystic or fatty degeneration
Metastasis	50	HU ≥ 10, however, cystic/necrotic changes can be < 10	Hypervascular metastases can washout in the adenoma range	RCC and HCC metastasis may show SI drop on opposed-phase imaging	In patient with a known malignancy, FDG PET has high sensitivity and specificity. Incidental adrenal metastasis from unknown malignancy is extremely rare
Lymphoma	43	HU ≥ 10, however, cystic/necrotic changes can be < 10	Variable attenuation and enhancement	NA	Usually PET FDG avid. Primary adrenal lymphoma is rare. Look for signs of lymphoproliferative disease elsewhere
Neuroblastoma	10–20	Calcifications	Variable attenuation and enhancement	NA	Usually MIBG avid. Tends to cross the midline and encase adjacent vessels Age (usually < 3–4 years) is a useful clue.
Pheochromocytoma	10	May simulate adenoma. Cystic and necrotic change can be ≤ 10 HU	Can washout in the adenoma range	No reported cases	Usually shows MIBG uptake. Consider associating syndromes
Myelolipoma	5–13	Macroscopic fat	NA	India ink outlining macroscopic fat on opposed-phase	May show calcifications or hemorrhage
Granulomatous infection	90	Variable, calcification	Variable	NA	Cystic/necrotic changes may mimic malignancy. Biopsy may be necessary
Hematoma	Usually unilateral	Variable depending on the stage of hemorrhage	No enhancement	Variable depending on the age of blood products	Clinical history of trauma, stress or bleeding tendency is usually helpful clue

Conclusion

Bilateral adrenal abnormalities can be manifested as masses (Table 1), enlargement, atrophy, or abnormal enhancement. Adrenal adenoma is the most common adrenal lesion and usually diagnosed confidently using non-enhanced CT, CS-MRI, or CT washout study. Adrenal metastasis and lymphoma can show variable and non-specific imaging features and both should be highly considered in the presence of a known primary malignancy or lymphoma. Pheochromocytoma and neuroblastoma are primary adrenal lesions that may present bilaterally, raising the possibility of familial or syndromic association. Both usually show MIBG uptake. Adrenal tuberculosis is usually bilateral and can mimic malignancy, necessitating adrenal biopsy in some instances. Adrenal hemorrhage can be bilateral and can present as mass-like adrenal lesion. Imaging features and clinical information are usually sufficient to diagnose adrenal hemorrhage. Adrenal enlargement usually, but not always, indicates underlying adrenal hyperplasia (Supplementary material: Algorithm 1). Adrenal atrophy suggests adrenal insufficiency, and is likely a sequel of prior granulomatous disease when associated with adrenal calcifications. Intense diffuse adrenal enhancement should raise the possibility of hypoperfusion complex. Adrenal enlargement with reduced or absent adrenal enhancement may suggest adrenal infarct in high-risk patients. Bilateral adrenal enlargement and diffuse predominantly peripheral calcifications are classic imaging findings of Wolman's disease.

Compliance with ethical standards

Conflict of interest All authors declare that they have no conflict of interest.

Ethical approval This study was not supported by grant funding. All procedures performed in studies involving human participants were in accordance with the ethical standards of the institutional research committee and with the 1964 Helsinki declaration and its later amendments or comparable ethical standards.

Informed consent Informed consent was not obtained for this retrospective review.

References

1. Kloos RT, Gross MD, Francis IR, Korobkin M, Shapiro B (1995) Incidentally discovered adrenal masses. Endocr Rev 16(4):460–484
2. Mansmann G, Lau J, Balk E, et al. (2004) The clinically inapparent adrenal mass: update in diagnosis and management. Endocr Rev 25(2):309–340
3. Song JH, Chaudhry FS, Mayo-Smith WW (2008) The incidental adrenal mass on CT: prevalence of adrenal disease in 1,049 consecutive adrenal masses in patients with no known malignancy. AJR Am J Roentgenol 190(5):1163–1168
4. Zeiger MA, Siegelman SS, Hamrahian AH (2011) Medical and surgical evaluation and treatment of adrenal incidentalomas. J Clin Endocrinol Metab 96(7):2004–2015
5. Pasternak JD, Seib CD, Seiser N, et al. (2015) Differences between bilateral adrenal incidentalomas and unilateral lesions. JAMA Surg 150(10):974–978
6. Muth A, Hammarstedt L, Hellstrom M, et al. (2011) Cohort study of patients with adrenal lesions discovered incidentally. Br J Surg 98(10):1383–1391
7. Zhou J, Ye D, Wu M, et al. (2009) Bilateral adrenal tumor: causes and clinical features in eighteen cases. Int Urol Nephrol 41(3):547–551
8. Gupta P, Bhalla A, Sharma R (2012) Bilateral adrenal lesions. J Med Imaging Radiat Oncol 56(6):636–645
9. Lomte N, Bandgar T, Khare S, et al. (2016) Bilateral adrenal masses: a single-centre experience. Endocr Connect 5(2):92–100
10. Johnson PT, Horton KM, Fishman EK (2009) Adrenal imaging with multidetector CT: evidence-based protocol optimization and interpretative practice. Radiographics 29(5):1319–1331
11. Choyke PL, Doppman JL (2000) Case 18: adrenocorticotropic hormone-dependent Cushing syndrome. Radiology 214(1):195–198
12. Siegelman ES (2012) Adrenal MRI: techniques and clinical applications. J Magn Reson Imaging 36(2):272–285
13. Kahn SL, Angle JF (2010) Adrenal vein sampling. Tech Vasc Interv Radiol 13(2):110–125
14. Taffel M, Haji-Momenian S, Nikolaidis P, Miller FH (2012) Adrenal imaging: a comprehensive review. Radiol Clin North Am 50(2):219–243
15. Schieda N, Siegelman ES (2017) Update on CT and MRI of adrenal nodules. AJR Am J Roentgenol 208(6):1206–1217
16. Boland GW, Lee MJ, Gazelle GS, et al. (1998) Characterization of adrenal masses using unenhanced CT: an analysis of the CT literature. AJR Am J Roentgenol 171(1):201–204
17. Korobkin M, Giordano TJ, Brodeur FJ, et al. (1996) Adrenal adenomas: relationship between histologic lipid and CT and MR findings. Radiology 200(3):743–747
18. Caoili EM, Korobkin M, Francis IR, Cohan RH, Dunnick NR (2000) Delayed enhanced CT of lipid-poor adrenal adenomas. AJR Am J Roentgenol 175(5):1411–1415
19. Tariq U, Poder L, Carlson D, et al. (2012) Multimodality imaging of fat-containing adrenal metastasis from hepatocellular carcinoma. Clin Nucl Med 37(6):e157–e159
20. Choi YA, Kim CK, Park BK, Kim B (2013) Evaluation of adrenal metastases from renal cell carcinoma and hepatocellular carcinoma: use of delayed contrast-enhanced CT. Radiology 266(2):514–520
21. Moosavi B, Shabana WM, El-Khodary M, et al. (2016) Intracellular lipid in clear cell renal cell carcinoma tumor thrombus and metastases detected by chemical shift (in and opposed phase) MRI: radiologic–pathologic correlation. Acta Radiol 57(2):241–248
22. Lam KY, Lo CY (2002) Metastatic tumours of the adrenal glands: a 30-year experience in a teaching hospital. Clin Endocrinol 56(1):95–101
23. Sasaguri K, Takahashi N, Takeuchi M, et al. (2016) Differentiation of benign from metastatic adrenal masses in patients with renal cell carcinoma on contrast-enhanced CT. AJR Am J Roentgenol 207(5):1031–1038
24. Schieda N, Krishna S, McInnes MDF, et al. (2017) Utility of MRI to differentiate clear cell renal cell carcinoma adrenal metastases from adrenal adenomas. AJR Am J Roentgenol 209(3):W152–W159
25. Tsushima Y, Takahashi-Taketomi A, Endo K (2009) Diagnostic utility of diffusion-weighted MR imaging and apparent diffusion coefficient value for the diagnosis of adrenal tumors. J Magn Reson Imaging 29(1):112–117
26. Vikram R, Yeung HD, Macapinlac HA, Iyer RB (2008) Utility of PET/CT in differentiating benign from malignant adrenal nodules in patients with cancer. AJR Am J Roentgenol 191(5):1545–1551
27. Boland GW, Blake MA, Holalkere NS, Hahn PF (2009) PET/CT for the characterization of adrenal masses in patients with cancer: qualitative versus quantitative accuracy in 150 consecutive patients. AJR Am J Roentgenol 192(4):956–962
28. Singh D, Kumar L, Sharma A, et al. (2004) Adrenal involvement in non-Hodgkin's lymphoma: four cases and review of literature. Leuk Lymphoma 45(4):789–794
29. Zhou L, Peng W, Wang C, et al. (2012) Primary adrenal lymphoma: radiological; pathological, clinical correlation. Eur J Radiol 81(3):401–405
30. Paling MR, Williamson BR (1983) Adrenal involvement in non-Hodgkin lymphoma. AJR Am J Roentgenol 141(2):303–305
31. Kato H, Itami J, Shiina T, et al. (1996) MR imaging of primary adrenal lymphoma. Clin Imaging 20(2):126–128
32. Metser U, Miller E, Lerman H, et al. (2006) 18F-FDG PET/CT in the evaluation of adrenal masses. J Nucl Med 47(1):32–37
33. Lo Cunsolo C, Casciano I, Gambini C, et al. (2001) Molecular alterations in a case of bilateral adrenal neuroblastoma. Med Pediatr Oncol 36(4):491–493
34. Schleiermacher G, Rubie H, Hartmann O, et al. (2003) Treatment of stage 4s neuroblastoma—report of 10 years' experience of the French Society of Paediatric Oncology (SFOP). Br J Cancer 89(3):470–476
35. Hiorns MP, Owens CM (2001) Radiology of neuroblastoma in children. Eur Radiol 11(10):2071–2081
36. Amar L, Bertherat J, Baudin E, et al. (2005) Genetic testing in pheochromocytoma or functional paraganglioma. J Clin Oncol 23(34):8812–8818
37. Caoili EM, Korobkin M, Francis IR, et al. (2002) Adrenal masses: characterization with combined unenhanced and delayed enhanced CT. Radiology 222(3):629–633
38. Blake MA, Kalra MK, Maher MM, et al. (2004) Pheochromocytoma: an imaging chameleon. Radiographics 24(1):S87–S99
39. Blake MA, Krishnamoorthy SK, Boland GW, et al. (2003) Low-density pheochromocytoma on CT: a mimicker of adrenal adenoma. AJR Am J Roentgenol 181(6):1663–1668
40. Rozovsky K, Koplewitz BZ, Krausz Y, et al. (2008) Added value of SPECT/CT for correlation of MIBG scintigraphy and diagnostic CT in neuroblastoma and pheochromocytoma. AJR Am J Roentgenol 190(4):1085–1090
41. Han M, Burnett AL, Fishman EK, Marshall FF (1997) The natural history and treatment of adrenal myelolipoma. J Urol 157(4):1213–1216
42. Kalidindi RS, Hattingh L (2006) Bilateral giant adrenal myelolipomas. Abdom Imaging 31(1):125–127
43. Kenney PJ, Wagner BJ, Rao P, Heffess CS (1998) Myelolipoma: CT and pathologic features. Radiology 208(1):87–95
44. Zhang HM, Perrier ND, Grubbs EG, et al. (2012) CT features and quantification of the characteristics of adrenocortical carcinomas on unenhanced and contrast-enhanced studies. Clin Radiol 67(1):38–46
45. Otal P, Escourrou G, Mazerolles C, et al. (1999) Imaging features of uncommon adrenal masses with histopathologic correlation. Radiographics 19(3):569–581
46. Guo YK, Yang ZG, Li Y, et al. (2007) Addison's disease due to adrenal tuberculosis: contrast-enhanced CT features and clinical duration correlation. Eur J Radiol 62(1):126–131
47. Wang YX, Chen CR, He GX, Tang AR (1998) CT findings of adrenal glands in patients with tuberculous Addison's disease. J Belge Radiol 81(5):226–228
48. Efremidis SC, Harsoulis F, Douma S, et al. (1996) Adrenal insufficiency with enlarged adrenals. Abdom Imaging 21(2):168–171
49. Yang ZG, Guo YK, Li Y, et al. (2006) Differentiation between tuberculosis and primary tumors in the adrenal gland: evaluation with contrast-enhanced CT. Eur Radiol 16(9):2031–2036
50. Vita JA, Silverberg SJ, Goland RS, Austin JH, Knowlton AI (1985) Clinical clues to the cause of Addison's disease. Am J Med 78(3):461–466
51. Kelestimur F, Unlu Y, Ozesmi M, Tolu I (1994) A hormonal and radiological evaluation of adrenal gland in patients with acute or chronic pulmonary tuberculosis. Clin Endocrinol 41(1):53–56

52. Kumar N, Singh S, Govil S (2003) Adrenal histoplasmosis: clinical presentation and imaging features in nine cases. Abdom Imaging 28(5):703–708
53. Kawashima A, Sandler CM, Ernst RD, et al. (1999) Imaging of nontraumatic hemorrhage of the adrenal gland. Radiographics 19(4):949–963
54. Rana AI, Kenney PJ, Lockhart ME, et al. (2004) Adrenal gland hematomas in trauma patients. Radiology 230(3):669–675
55. Jordan E, Poder L, Courtier J, et al. (2012) Imaging of nontraumatic adrenal hemorrhage. AJR Am J Roentgenol 199(1):W91–W98
56. Tan GX, Sutherland T (2016) Adrenal congestion preceding adrenal hemorrhage on CT imaging: a case series. Abdom Radiol 41(2):303–310
57. Aljabri KS, Bokhari SA, Alkeraithi M (2011) Adrenal hemangioma in a 19-year-old female. Ann Saudi Med 31(4):421–423
58. Young SA, Shapiro B (1998) Klippel-Trenaunay-Weber syndrome with adrenal pseudocyst: characterization by blood pool and adrenocortical iodocholesterol scintigraphy. Clin Nucl Med 23(8):528–531
59. Ojili V, Tirumani SH, Gunabushanam G, et al. (2013) Abdominal hemangiomas: a pictorial review of unusual, atypical, and rare types. Can Assoc Radiol J 64(1):18–27
60. Doppman JL, Gill JR Jr, Nienhuis AW, Earll JM, Long JA Jr (1982) CT findings in Addison's disease. J Comput Assist Tomogr 6(4):757–761
61. Sohaib SA, Hanson JA, Newell-Price JD, et al. (1999) CT appearance of the adrenal glands in adrenocorticotrophic hormone-dependent Cushing's syndrome. AJR Am J Roentgenol 172(4):997–1002
62. Lingam RK, Sohaib SA, Vlahos I, et al. (2003) CT of primary hyperaldosteronism (Conn's syndrome): the value of measuring the adrenal gland. AJR Am J Roentgenol 181(3):843–849
63. Rockall AG, Babar SA, Sohaib SA, et al. (2004) CT and MR imaging of the adrenal glands in ACTH-independent cushing syndrome. Radiographics 24(2):435–452
64. Michelle MA, Jensen CT, Habra MA, et al. (2017) Adrenal cortical hyperplasia: diagnostic workup, subtypes, imaging features and mimics. Br J Radiol 90(1079):14
65. Verma A, Mohan S, Gupta A (2008) ACTH-independent macronodular adrenal hyperplasia: imaging findings of a rare condition: a case report. Abdom Imaging 33(2):225–229
66. Kawashima A, Sandler CM, Fishman EK, et al. (1998) Spectrum of CT findings in nonmalignant disease of the adrenal gland. Radiographics 18(2):393–412
67. Al Essa M, Nounou R, Sakati N, et al. (1998) Wolman's disease: the King Faisal Specialist Hospital and Research Centre experience. Ann Saudi Med 18(2):120–124
68. Sen D, Satija L, Saxena S, Rastogi V, Singh M (2015) A rare constellation of imaging findings in Wolman disease. Med J Armed Forces India 71(Suppl 2):26
69. Westra SJ, Zaninovic AC, Hall TR, Kangarloo H, Boechat MI (1994) Imaging of the adrenal gland in children. Radiographics 14(6):1323–1340
70. O'Hara SM, Donnelly LF (1999) Intense contrast enhancement of the adrenal glands: another abdominal CT finding associated with hypoperfusion complex in children. AJR Am J Roentgenol 173(4):995–997
71. Espinosa G, Santos E, Cervera R, et al. (2003) Adrenal involvement in the antiphospholipid syndrome: clinical and immunologic characteristics of 86 patients. Medicine 82(2):106–118
72. Inam S, Sidki K, al-Marshedy AR, Judzewitsch R (1991) Addison's disease, hypertension, renal and hepatic microthrombosis in 'primary' antiphospholipid syndrome. Postgrad Med J 67(786):385–388
73. Riddell AM, Khalili K (2004) Sequential adrenal infarction without MRI-detectable hemorrhage in primary antiphospholipid–antibody syndrome. AJR Am J Roentgenol 183(1):220–222
74. Ames DE, Asherson RA, Ayres B, Cassar J, Hughes GR (1992) Bilateral adrenal infarction, hypoadrenalism and splinter haemorrhages in the 'primary' antiphospholipid syndrome. Br J Rheumatol 31(2):117–120